iScience

CellPress
OPEN ACCESS

Article

Mechanism underlying follicular hyperproliferation and oncogenesis in hidradenitis suppurativa

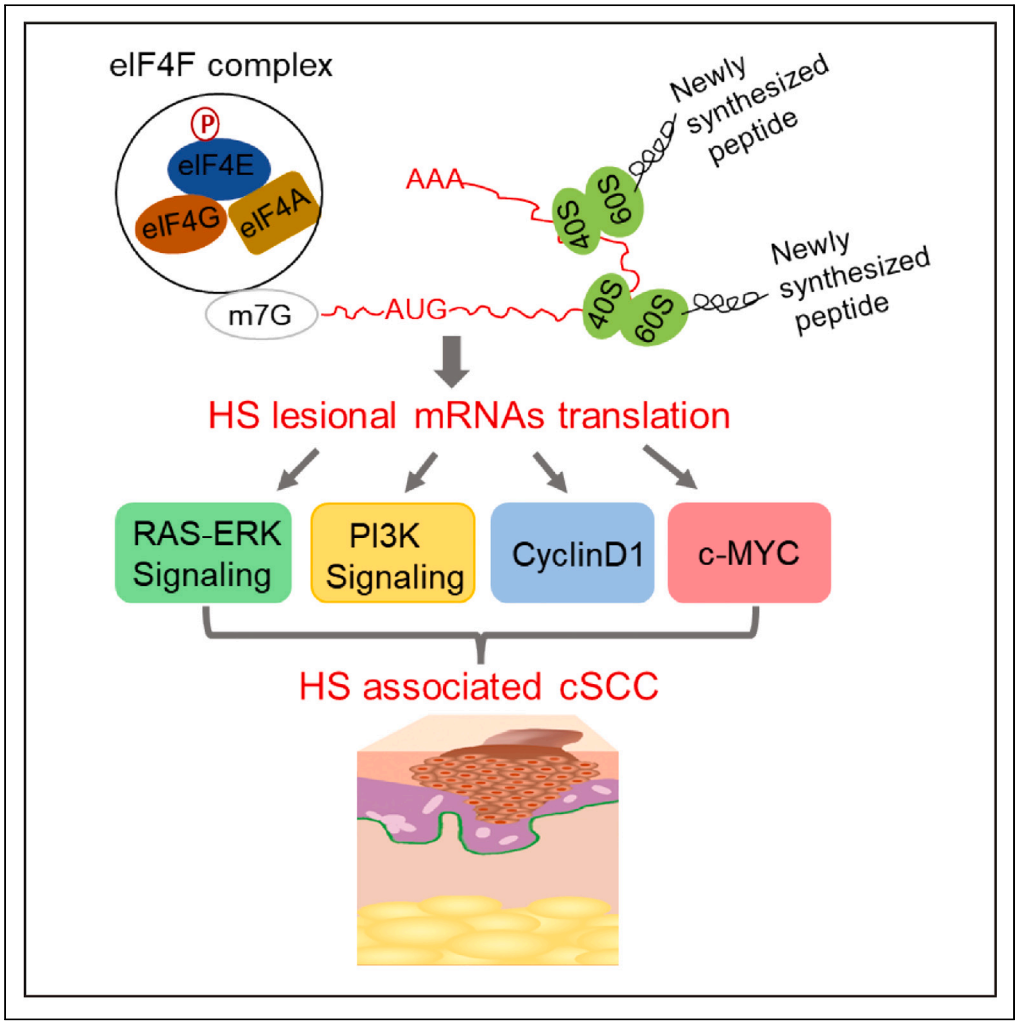

Lin Jin, Mahendra P. Kashyap, Yunjia Chen, ..., Boni E. Elewski, Craig A. Elmets, Mohammad Athar

mohammadathar@uabmc.edu

Highlights

eIF4F is associated with follicular hyperproliferation in HS

eIF4F targets Cyclin D1 and c-MYC are highly expressed activating Ras, PI3K, and ERK

The interplay of Cyclin D1 and c-MYC is associated with HS-related KA pathogenesis

nCyclin D1-CDK4 expressed throughout KA lesions providing oncogenic signaling

Jin et al., iScience 26, 106896
June 16, 2023
https://doi.org/10.1016/j.isci.2023.106896

iScience

CellPress
OPEN ACCESS

Article

Mechanism underlying follicular hyperproliferation and oncogenesis in hidradenitis suppurativa

Lin Jin,[1,2,3] Mahendra P. Kashyap,[2,3] Yunjia Chen,[4] Jasim Khan,[2,3] Yuanyuan Guo,[2,3] Jari Q. Chen,[5] Madison B. Lee,[6] Zhiping Weng,[1,2,3] Allen Oak,[2,11] Prasanth Patcha,[7] Tiffany Mayo,[2] Rajesh Sinha,[2,3] Venkatram Atigadda,[2] Shahid M. Mukhtar,[8] Jessy S. Deshane,[9] Chander Raman,[2] Carly Elston,[10] Boni E. Elewski,[2] Craig A. Elmets,[2] and Mohammad Athar[1,2,3,12,*]

SUMMARY

Hidradenitis suppurativa (HS) is a skin disorder that causes chronic painful inflammation and hyperproliferation, often with the comorbidity of invasive keratoacanthoma (KA). Our research, employing high-resolution immunofluorescence and data science approaches together with confirmatory molecular analysis, has identified that the 5′-cap-dependent protein translation regulatory complex eIF4F is a key factor in the development of HS and is responsible for regulating follicular hyperproliferation. Specifically, eIF4F translational targets, Cyclin D1 and c-MYC, orchestrate the development of HS-associated KA. Although eIF4F and *p*-eIF4E are contiguous throughout HS lesions, Cyclin D1 and c-MYC have unique spatial localization and functions. The keratin-filled crater of KA is formed by nuclear c-MYC-induced differentiation of epithelial cells, whereas the co-localization of c-MYC and Cyclin D1 provides oncogenic transformation by activating RAS, PI3K, and ERK pathways. In sum, we have revealed a novel mechanism underlying HS pathogenesis of follicular hyperproliferation and the development of HS-associated invasive KA.

INTRODUCTION

Hidradenitis suppurativa (HS) is a chronic, recurrent, inflammatory skin disease often associated with painful and distressing symptoms.[1,2] HS primarily affects apocrine gland–rich regions of the body such as the axillary, inguinal, and anogenital areas. Young adults of age 20 to 40 years have the highest incidence rates (0.05–4%), and women are more frequently affected than men.[3,4] Patients with the progressive disease develop inflammatory nodules, abscesses, and tunnels under the skin. HS severity is classified with the Hurley staging system: Stage I is the mildest, stage II is intermediate, and stage III is the most severe.[5] Although several risk factors including inherited genetic mutations, hormonal status, obesity, and smoking are known to be associated with disease severity, the molecular drivers of HS are largely unknown.[6] Until now, surgical treatment remains the ultimate option for patients with Hurley late stage II and stage III disease.[7,8] Comorbidity studies have found that HS patients have a significantly increased risk of many disorders including that of cutaneous squamous cell carcinoma (cSCC).[9–13] The exact mechanism by which HS-associated epithelial keratinocytes are transformed into cSCC remains unknown.

Increased protein synthesis, coupled with increased ribosome number, is necessary for cells to transition from quiescence to proliferation, which is considered an important step in hyperproliferative disease and in tumor progression.[14] Translational control aberrantly dysregulates the cell cycle and proliferation. In this regard, a heterogeneous protein complex (also known as eIF4F) comprising eIF4E, eIF4G, and eIF4A1 proteins binds to the 5′-cap of messenger RNAs (mRNAs). eIF4E is the rate-limiting factor for 5′-cap-dependent translation initiation and, thus, is an important rate-limiting regulator of protein translation initiation.[15] The function of eIF4E is regulated by its availability and is controlled by the 4E-BPs via phosphorylation at Ser-209, which is mediated by the eIF4G-associated kinases, the MAPK-interacting protein kinase (MNK)1 and MNK2.[16] In addition, mTOR is important in this process as it regulates the phosphorylation of 4E-BPs and consequent binding of eIF4E within the eIF4F complex.[17] Although the

[1]Center for Epigenomics and Translational Research in Inflammatory Skin Diseases, University of Alabama at Birmingham, Birmingham, AL 35294, USA

[2]Department of Dermatology, School of Medicine, University of Alabama at Birmingham, Birmingham, AL 35294, USA

[3]UAB Research Center of Excellence in Arsenicals, University of Alabama at Birmingham, Birmingham, AL 35294, USA

[4]Department of Genetics, University of Alabama at Birmingham, Birmingham, AL 35294, USA

[5]Hoover High School, Hoover, Birmingham, AL 35244, USA

[6]School of Medicine, University of Alabama at Birmingham, Birmingham, AL 35294, USA

[7]Division of Plastic Surgery, University of Alabama at Birmingham, Birmingham, AL 35294, USA

[8]Department of Biology, University of Alabama at Birmingham, Birmingham, AL 35294, USA

[9]Division of Pulmonary, Allergy and Critical Care Medicine, University of Alabama at Birmingham, Birmingham, AL 35294, USA

[10]Department of Dermatology and Dermatopathology, University of Alabama at Birmingham, Birmingham, AL 35294, USA

[11]Present address: Department of Dermatology, University of Pennsylvania

Continued

pathologic role of 5′-cap translation is also known in cancers,[18] its involvement in the pathogenesis of HS remains undescribed. We recently reported that increased expression of phosphorylated eIF4E, eIF4G, and eIF4A1 is associated with UVB-induced human and murine skin cSCC.[19]

The elevated expression and aberrant activity of the eIF4F complex involve selective translation of mRNAs needed for proliferation, metastasis, and multidrug resistance in tumor growth.[20–22] Disruption of the eIF4 complex formation either by blocking the eIF4E-eIF4G interaction or by targeting eIF4A can pause cell cycle progression, which is followed by induction of apoptosis in cancer cells and may thus provide a therapeutic strategy.[18,19,23]

In this study, we demonstrate the involvement of aberrant protein translation control in the pathogenesis of HS and contiguous cSCCs. We observed increased and widespread expression of eIF4E/eIF4A1/eIF4G proteins in HS follicular hyperproliferation regions of the skin and HS-associated cSCC. The two key translational targets of eIF4F, Cyclin D1, and c-MYC, were enhanced and showed pathogenesis-related spatial distribution. Moreover, eIF4F-associated RAS and PI3K oncogene signaling networks are highly enriched in HS transcriptome and their integration may contribute to transcriptional amplification of c-MYC. The c-MYC expression alone in specific epithelial cells juxtaposed to the crater of KA provided a key mechanism underlying the differentiation, whereas co-localization of c-MYC with Cyclin D1 in the nucleus of epithelial cells promotes their transformation to invasive KA. Collectively, our work provides a novel insight into the role of the eIF4F complex in chronic severe HS disease and underscores a possible mechanism for the oncogenic activity of HS epithelial cells. Inhibition of eIF4F would open new avenues for the therapeutic intervention of HS lesions and HS-associated aggressive and lethal cSCC.

RESULTS

eIF4F complex proteins highly expressed in HS skin

Consistent with earlier observations, we found follicular hyperplasia and massive infiltration of inflammatory cells in HS skin (Figure 1A). To identify molecular triggers in HS pathogenesis, we assessed the expression and distribution of proteins associated with the eIF4 complex namely eIF4A1, eIF4E, and eIF4G. Although a slight to moderate expression of eIF4A1 and eIF4G was mainly observed in the basal layer of the epidermis of healthy skin, high expression of eIF4E was noted in the basal and suprabasal epidermis (Figure 1B, upper). In contrast, high expression of eIF4A1/4E/4G expression characterized the hyperplastic follicular epithelium in HS. Of interest, eIF4A1/4E/4G was also present throughout the dermal compartment (Figure 1B, middle and bottom). Overall, these three proteins were more widely distributed in HS skin than in healthy skin (Figure 1C). In keratinocytes of both healthy and HS skin, eIF4A1 and eIF4G were mainly expressed in the cytoplasm; however, eIF4E protein localized to both the cytoplasm and the nucleus, which is consistent with its suggested role in exporting mRNA from the nucleus to cytosol.[15] The high expression of eIF4F complex proteins both in hyperplastic epithelia and hypodermal components of the skin suggests its importance in the progression of HS lesions (Figure 1D). In western blot analysis, the expression of the overall expression of eIF4E/4A1/4G and phosphorylated eIF4E were also significantly elevated in HS skin (Figures 1E and 1F).

Sub-tissue anatomical localization of eIF4E/eIF4A1/eIF4G in HS skin

eIF4F complex in the cytoplasm of eukaryotes has previously been reported to be important for translation initiation.[24] To explore the profile and sub-tissue localization of different eIF4F components in HS keratinocytes, we utilized IF staining followed by confocal microscopy to capture high-resolution images. In healthy skin, weak signals for eIF4A1, eIF4E, and eIF4G, were confined mainly to the basal epidermal layer, which progressively diminished through the differentiated layers (Figures 2A and S1). In HS skin, eIF4E and eIF4G were widespread throughout the hyperproliferative compartment (Figures 2B and 2C, i and ii), and their co-localization was enhanced as shown by their mutually overlapping co-localization signals (Figure S1) from the basal to suprabasal layers. eIF4A1 staining was mainly observed in the hyperproliferative suprabasal layers as well as within the multiple tunnels of the sinus tract (Figures 2B and 2C, iii). The merged immunoreactivity demonstrated by bright overlapping signals all over the tunnel-forming cells suggests a role of eIF4F in the development of multiple tunnels characterizing late-stage disease (Figures 2B and 2C, iv). The eIF4G and eIF4A1 staining was predominantly cytoplasmic (Figure 2C, ii and iii). In contrast, immunofluorescence signals for eIF4E were observed in both the cytoplasm and nucleus (Figure 2C, i), which is consistent with our IHC results (Figure 1B). Collectively, these results reveal eIF4F complex proteins assemble as a ternary complex within the cytoplasm of keratinocytes in HS, which then aberrantly reprograms translation for genes regulating hyperproliferation, differentiation, and keratinization in HS skin.

School of Medicine, Philadelphia, PA 19104, USA

[12]Lead contact

*Correspondence: mohammadathar@uabmc.edu

https://doi.org/10.1016/j.isci.2023.106896

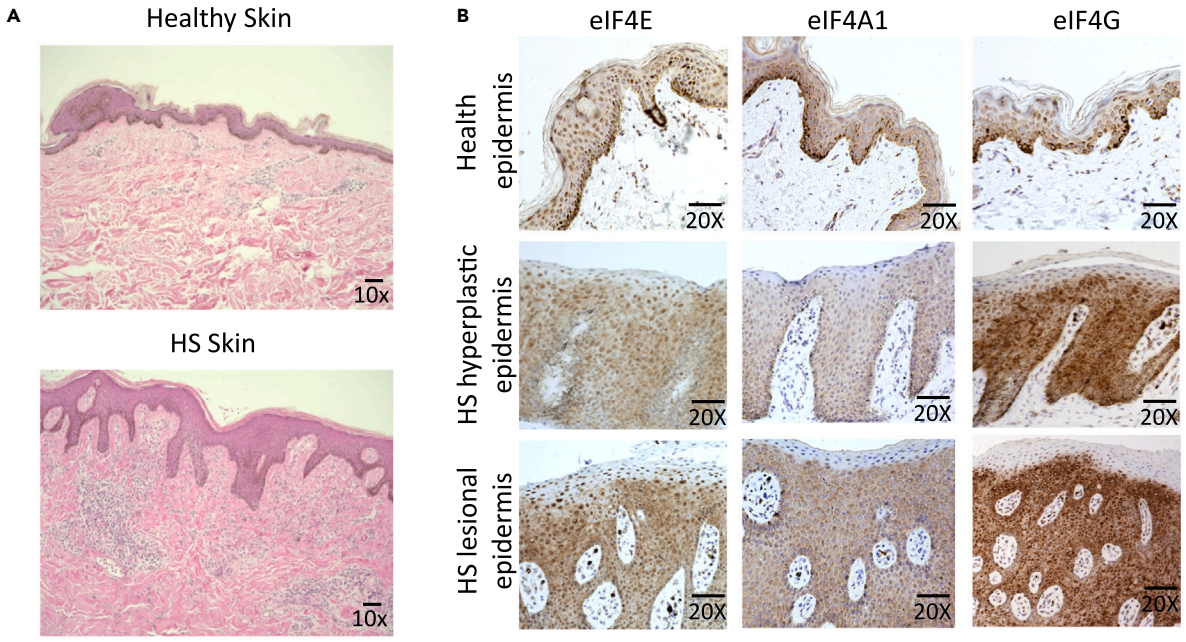
A
Healthy Skin
10x
HS Skin
10x
B
eIF4E
eIF4A1
eIF4G
Health epidermis
HS hyperplastic epidermis
HS lesional epidermis
20X

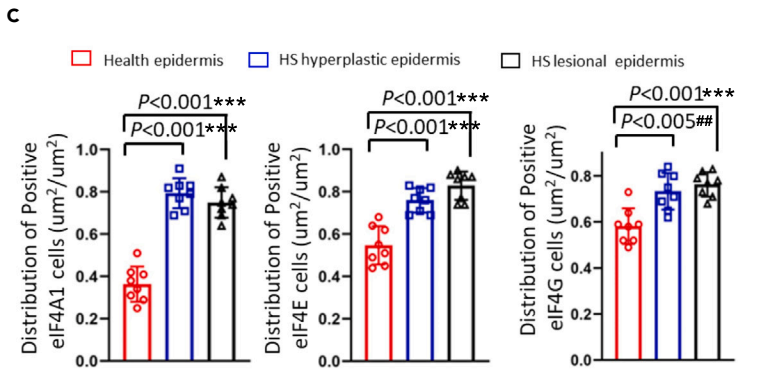
C
Health epidermis
HS hyperplastic epidermis
HS lesional epidermis
Distribution of Positive eIF4A1 cells (um²/um²)
Distribution of Positive eIF4E cells (um²/um²)
Distribution of Positive eIF4G cells (um²/um²)
P<0.001***
P<0.005##

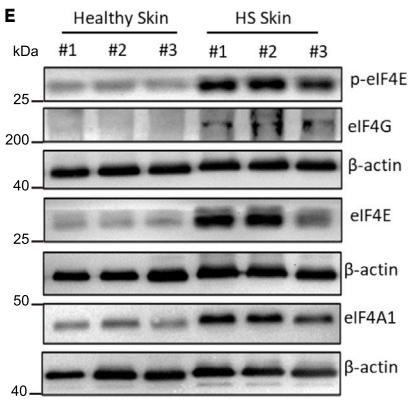
E
Healthy Skin
HS Skin
kDa
#1
#2
#3
p-eIF4E
eIF4G
β-actin
eIF4E
β-actin
eIF4A1
β-actin

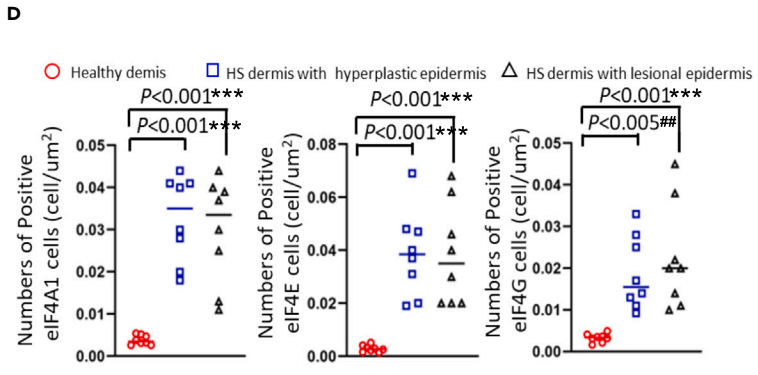
D
Healthy demis
HS dermis with hyperplastic epidermis
HS dermis with lesional epidermis
Numbers of Positive eIF4A1 cells (cell/um²)
Numbers of Positive eIF4E cells (cell/um²)
Numbers of Positive eIF4G cells (cell/um²)
P<0.001***
P<0.005##

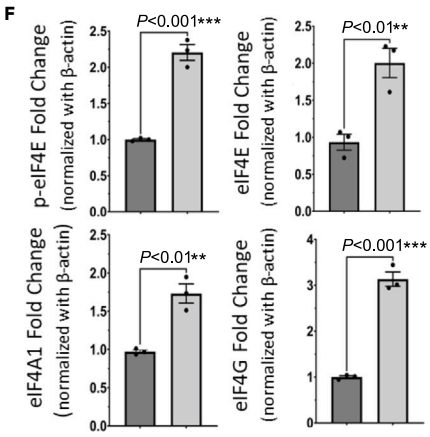
F
p-eIF4E Fold Change (normalized with β-actin)
eIF4E Fold Change (normalized with β-actin)
eIF4A1 Fold Change (normalized with β-actin)
eIF4G Fold Change (normalized with β-actin)
P<0.001***
P<0.01**

Figure 1. Protein expression analysis of eIF4E/eIF4A1/eIF4G in HS skin

(A) Representative H&E staining of human healthy and HS skin. Scale bar = 50 μm.

(B) Representative images of human healthy and HS skin sections showing IHC staining for eIF4E, eIF4A1, and eIF4G proteins. Scale bar = 50 μm. The experiment was performed on 8 individuals for healthy and HS skin, respectively, and had similar results.

(C) Representative bar graphs showing the quantitative staining density of eIF4E, eIF4A1, and eIF4G, proteins in healthy and HS epidermis (n = 8 areas per sample). The experiment was repeated on 8 individuals for healthy and HS skin, respectively, and had similar results. The epidermal distribution of stained cells was assessed by the ratio of the area of positive cell layers to the area of total cell layers. Data are represented as mean ± standard error of the mean (SEM). p-values based on ANOVA test. $^{\#\#}p < 0.005$, $^{***}p < 0.001$.

(D) Graphs showing positive cell numbers for the indicated eIF4F complex proteins in healthy and HS dermis (n = 8 areas per group). The experiment was repeated on 8 individuals for healthy and HS skin, respectively, and had similar results. The number of positive cells per square micrometer was determined by manually counting stained cells from eight random fields per sample. Data are represented as mean ± SEM. p-values based on ANOVA test. $^{\#\#}p < 0.005$, $^{***}p < 0.001$.

(E) Western blot analysis of *p*-eIF4E, eIF4E, eIF4A1, and eIF4G, expression in human HS skin compared with those in healthy skin tissue (n = 3 individuals per group).

(F) Histogram showing densitometry analysis of band intensity and presented in fold change (n = 3 individuals per group). Data are represented as mean ± SEM. p-values based on unpaired two-tailed Student's *t* test. $^{**}p < 0.01$, $^{***}p < 0.001$.

Target genes signature of eIF4F complex in HS lesions

Using publicly available bulk RNA-seq datasets,[25] we performed gene ontology (GO) analysis of the non-lesional and lesional HS skin. Compared to healthy skin, differentially expressed genes (DEGs) in non-lesional skin are enriched in RNA and ATP binding, DNA repair, ubiquitin-protein ligase activity, and in the negative regulation of cell proliferation (Figure 3A). Whereas, in lesional skin, the major pathways enriched are G protein-coupled receptor signaling, defense response to the bacterium, calcium ion binding, and blood microparticle (Figure 3B). Both inflammatory and immune responses were found to be elicited in HS skin. Next, we sought to perform pairwise comparisons between the human HS transcriptome[25] and the core signature of eIF4A targets as identified in mouse tumor organoids.[26] There was a substantial overlap in DEGs, with a shared group of 734 genes that were differentially expressed in all three groups (Figure 3C; Table S1). Among those, 516 were upregulated and 218 were downregulated (Figure 3D). Therefore, this DEGs list served as a reference dataset for eIF4F target identification in HS. We profiled the top 50 upregulated and downregulated DEGs, respectively (Figure 3E). Genes overexpressed in HS (compared to healthy controls), including those with known involvement in tumorigenesis (*ACTRT3*, *CNN3*, and *PTPRN2*), skin inflammation (*IL10RA*, *CBARP*, and *PTAFR*), keratinization process (*CCR2* and *FLI1*), skin fibrosis (*DOCK10*), innate immunity (*TLR7* and *BTK*), as well as in keratinocyte growth and differentiation (*CRABP2*). However, enriched down-regulated genes represented Wnt signaling (*WNT2B* and *WLS*), cell adhesion (*ELFN2*), epidermal homeostasis mediator (*KLK1* and *WDR72*), and inflammatory modulators (*TPH1* and *CXCL14*). We also validated the relative abundance of transcription for some of the genes from the DEGs list using RT-qPCR (Figure 3F). Our results confirmed *MYO1G*, *TBX2*, and *LEF1*, were significantly upregulated; and *CXCL14* and *DLX1* were decreased.

Signaling pathways in HS lesional skin

Gene Ontology (GO) terms successfully enriched several biological processes, namely immune system-associated processes, inflammation, regulation of TNF production, and positive regulation of cell proliferation, including PI3K signaling (Figure 4A). To investigate whether the products of these gene transcripts are associated in the progression of HS, we performed relevant pathway enrichment analysis by mapping the results from 734 DEGs to the GSEA repository (Figure 4B). We found that the expression of genes involved in the inflammatory response and complement pathways was skewed toward HS disease progression. Specifically, interferon-gamma (IFN-γ) signaling was significantly upregulated in HS skin. Many of the genes in RAS and PI3K signaling pathways were also upregulated in HS. Key RAS/MEK/ERK and PI3K gene sets were further subjected to annotated hierarchical clustering procedures and presented as heatmaps. Among them, 33 genes in the RAS/MEK/ERK pathway were upregulated in HS, including those regulating cell growth (*KDR*, *IGF1*, and *PDGFRB*), NADPH oxidase complex (*NCF1* and *NOX4*), and inflammation (*IL6*) (Figure S2A). Fifteen genes upregulated in the PI3K pathway include those among the immune-related hub gene (*HCLS1*) (Figure S2B). We confirmed these results using western blot analysis for ERK signaling and two of the downstream effectors of the PI3K pathway that were significantly activated in HS skin (Figures 4C and 4D). Next, we performed an ingenuity pathway analysis (IPA) of the eIF4F-associated DEGs to identify the predicted activated upstream regulators in HS skin. IPA established a total of 20 functionally related gene hubs for 20 activated processes (Figure 4E). Major activated modules included inflammatory cytokines (*IL6*, *IL21*, *IL1B*, *TNF*, *CSF2*, and *IFNG*, and others), intra-cellular signal regulators (*NOTCH4* and *MAP2K1*), vascular endothelial growth

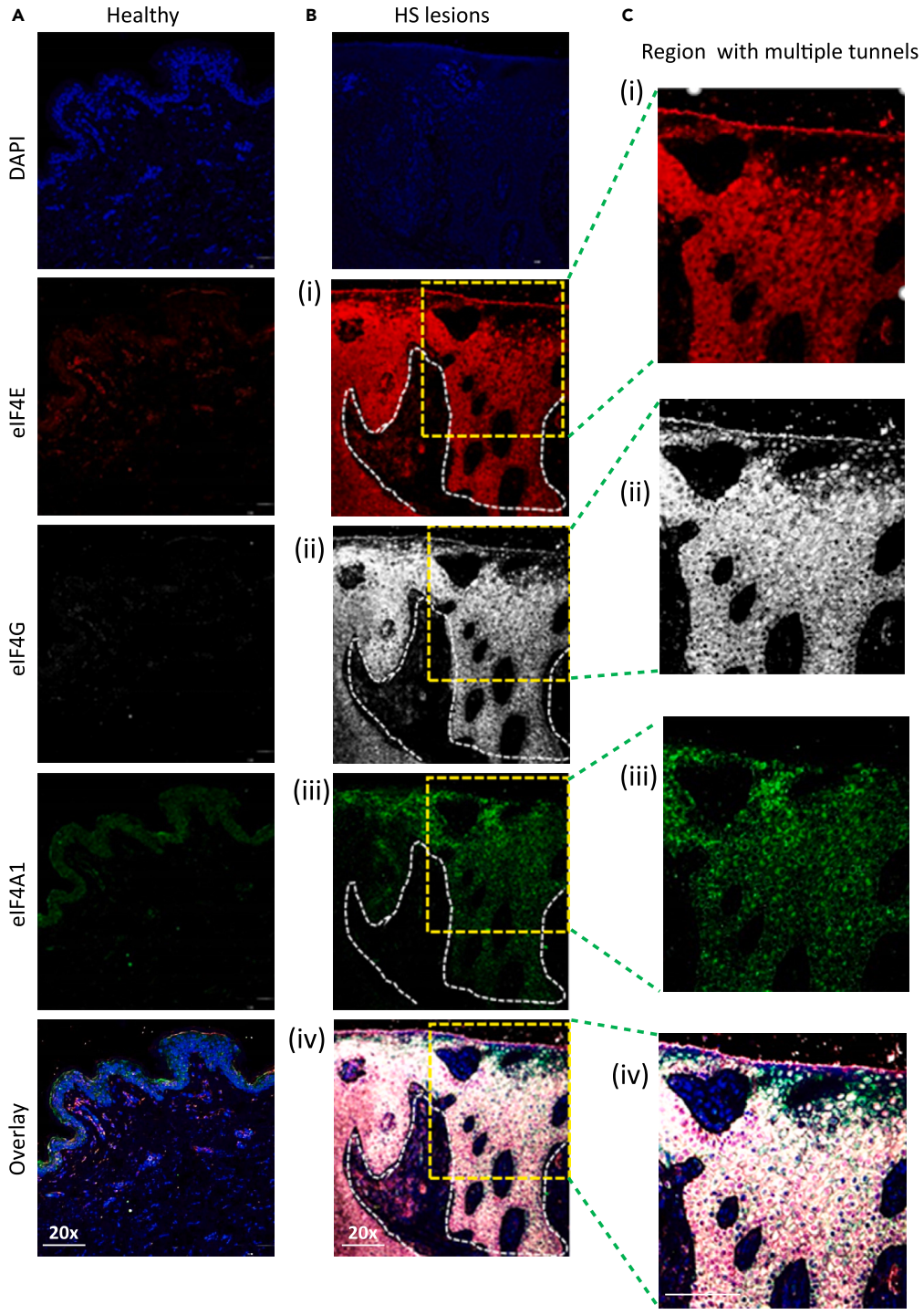

Figure 2. High-resolution confocal images of proteins expression for eIF4F components in HS lesions

(A and B) Representative images showing the expression of eIF4E (red), eIF4A1 (green), and eIF4G (gray), along with DAPI (blue), stained in nuclei in healthy human skin (A) and HS skin lesions (B). The experiment was repeated on 8 individuals for healthy and HS skin, respectively, and had similar results. White dot line indicates the junction of epidermal and dermal compartments. Scale bar = 100 μm.

(C) Zoom area (yellow dot line box) of images from (B). Scale bar = 100 μm.

See also Figures S1.

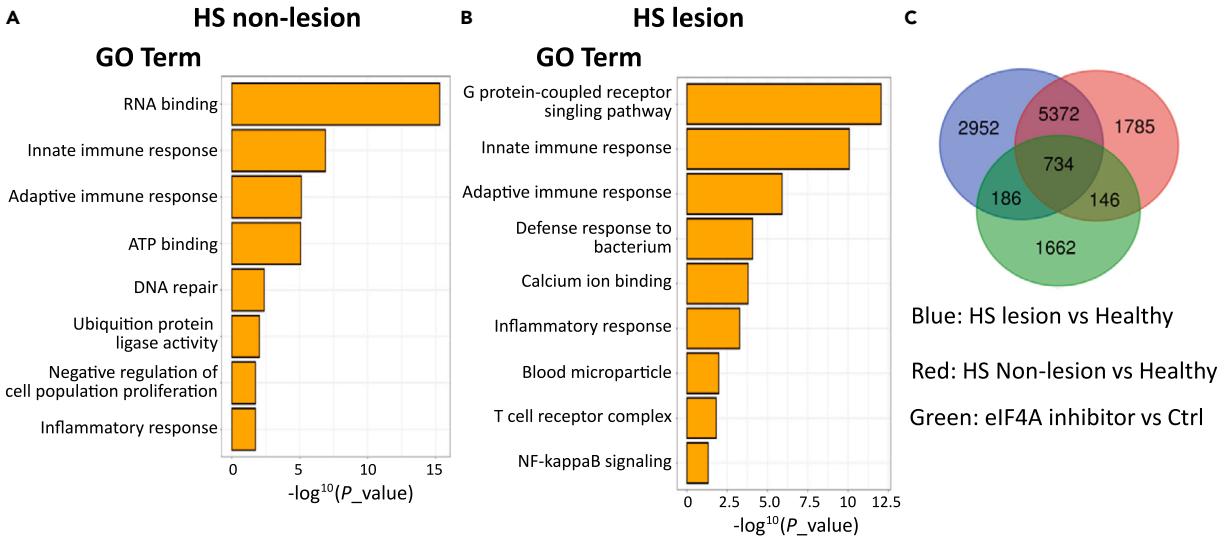
A
HS non-lesion
GO Term
RNA binding
Innate immune response
Adaptive immune response
ATP binding
DNA repair
Ubiquition protein ligase activity
Negative regulation of cell population proliferation
Inflammatory response
0
5
10
15
-log10(P_value)
B
HS lesion
GO Term
G protein-coupled receptor singling pathway
Innate immune response
Adaptive immune response
Defense response to bacterium
Calcium ion binding
Inflammatory response
Blood microparticle
T cell receptor complex
NF-kappaB signaling
0
2.5
5.0
7.5
10
12.5
-log10(P_value)
C
2952
5372
1785
734
186
146
1662
Blue: HS lesion vs Healthy
Red: HS Non-lesion vs Healthy
Green: eIF4A inhibitor vs Ctrl

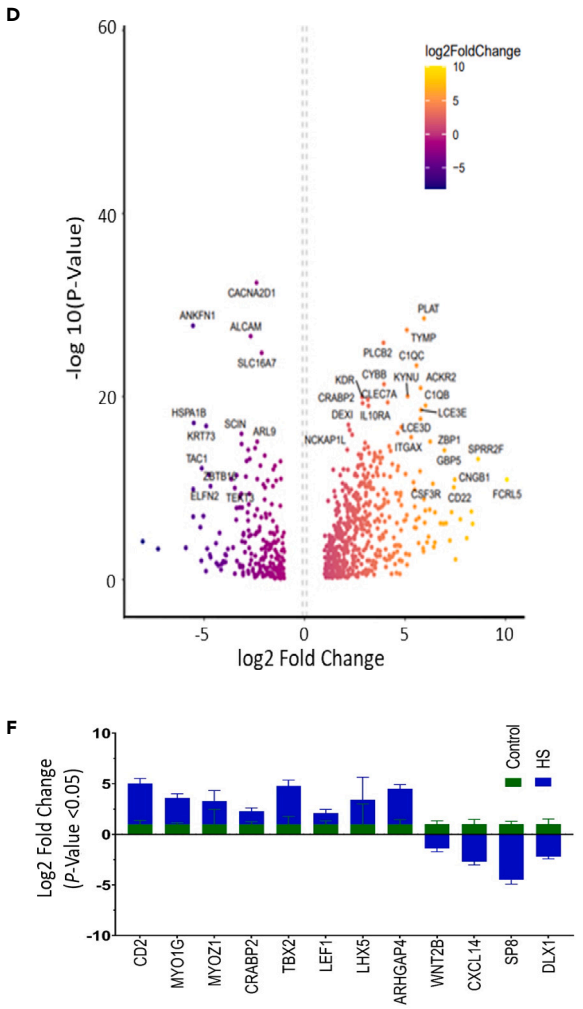
D
log2FoldChange
10
5
0
−5
-log 10(P-Value)
log2 Fold Change
CACNA2D1
ANKFN1
ALCAM
SLC16A7
HSPA1B
KRT73
SCIN
ARL9
TAC1
ZBTB16
ELFN2
TEKT3
PLAT
TYMP
PLCB2
C1QC
CYBB
KYNU
ACKR2
KDR
CLEC7A
C1QB
CRABP2
DEXI
IL10RA
LCE3E
LCE3D
NCKAP1L
ITGAX
ZBP1
SPRR2F
GBP5
CNGB1
CSF3R
CD22
FCRL5
E
z score
2
1
0
−1
Healthy1
Healthy2
Healthy3
Healthy4
HS1
HS2
HS3
HS4
HS5
HS6
HS7
FLT1
CCR2
ACTRT3
PTAFR
CRABP2
TLR7
BTK
DOCK10
PTPRN2
IL10RA
CBARP
CNN3
WNT2B
KLK1
ELFN2
WDR72
TPH1
CXCL14
F
Log2 Fold Change (P-Value <0.05)
Control
HS
CD2
MYO1G
MYOZ1
CRABP2
TBX2
LEF1
LHX5
ARHGAP4
WNT2B
CXCL14
SP8
DLX1

Figure 3. Analysis of target genes potentially regulated by eIF4F complex in HS skin

(A and B) GO enrichment analysis showing top 8–9 ranked biological functions for DEGs (GSE155176) in HS non-lesional (A) and lesional skin (B).

(C) Venn diagram showing the intersection of eIF4F target genes among human healthy, HS lesions, and HS non-lesions, transcriptome (GSE155176), and the core signature of eIF4A targets in mouse tumor organoids (GSE125380). The detailed number of overlapping genes derived from each comparison is shown inside the circles.

(D) Volcano plot showing DEGs potentially regulated by eIF4F in HS skin. The X axis represents the fold-change (log-scaled) and the Y axis represents the p-value (log-scaled). Each symbol represents a different gene. Genes with –log10 (p-value) $\geq$ 10 are indicated.

(E) Heatmap representation of the top 50 DEGs generated from Figure 4C. Representative gene names are displayed on a heatmap.

(F) qRT-PCR validation for selected genes from (A). Total RNA from healthy skin (n = 4) and HS skin (n = 7) was extracted, reverse transcribed, and analyzed. The Y axis represents the fold-change (log-scaled). GAPDH expression was used for normalization. Data are represented as mean $\pm$ SEM.

See also Table S1.

factor (*VEGFA*), immune signal transduction molecules (*ICAM1* and *MYD88*), and inflammation-associated transcription factors (*STAT1* and *RELA*). These modules were interconnected, which led to enhancing the recruitment of lymphocytes and mononuclear leukocytes as well as regulating the homeostasis of leukocytes. Repressed expression of regulators included *IKZF2* and *SOCS1*, which are known to play a role in T cell differentiation. Together, eIF4F-associated signals in HS skin regulated oncogenic signaling pathways, and inflammatory and immune processes, which create a conducive environment for promoting tumorigenesis in severe HS stage II/III patients.

RAS/MEK/ERK signals were highly enriched in our reference dataset for eIF4F targets. As they are crucial regulators of cell proliferation, differentiation, and cell survival as well as malignant transformation, we examined lists of genes encoding proteins required for cell proliferation and cell cycle. Increased expression of 105 genes associated with the proliferation in HS samples was identified (Figure S2C). Among them important to be mentioned are transcription factors (*STAT4*, *PAX1*, and *LHX5*) for epithelial cells, tyrosine kinase-related gene *TEK* for endothelial cells, forkhead family member *FOXF* for fibroblast cells, zinc finger protein *IKZF1* for T cells, transcription factor *LEF1* for B cells, and interleukin *IL12B* for natural killer cells (Figure S2D). We also found increased expression of a mitotic regulator, *FBXL7*, and a positive regulator of the cell cycle, *PROX1*, in HS samples (Figure S2E).

We performed the BrdU incorporation assay to compare the proliferative capacity of epidermal cells under normal and HS conditions. The epidermal cells isolated from HS skin manifested significantly enhanced BrdU incorporation compared to healthy counterparts (Figure 5A), confirming the presence of actively proliferating epithelial cells in HS lesional epithelium. To further identify and quantify cells that entered the proliferative state, we also assessed the relative number of cells at different stages in the cell cycle by flow cytometry following BrdU labeling. A significantly higher number of HS lesional epithelial cells were in the 'S' phase as compared to those in healthy controls, suggesting an augmented DNA synthesis in HS skin cells (Figure 5B). In our *ex vivo* validation, we consistently observed that HS-lesional keratinocytes had enhanced proliferation capacity compared to those from healthy skin (Figure 5C).

Elevated expression of nuclear Cyclin D1 and c-MYC in HS epithelia

We investigated the expression levels of Cyclin D1 and c-MYC as eIF4F target proteins, the known key players in epidermal differentiation, proliferation, and oncogenic transformation. Consistent with previous observations in healthy skin, Cyclin D1 accumulated in the cytoplasm of cells within the stratified epidermal layer (Figure 6A and S3A). In line with the known role of c-MYC in keratinocyte differentiation,[27] high expression of c-MYC was more prominent within differentiated layers of the epidermis and was almost absent in the basal layer of the epidermis (Figure S3A). The nuclear localization of c-MYC was found throughout the lesional epidermis (Figures 6B and S3B). Strong co-localization signal for Cyclin D1 and c-MYC was found mainly in most of the peripheral epithelial cells forming tunnels (Figure 6B, right bottom, and 6C; Figure S3B). This specific subpopulation of cells expressing the two potent oncoproteins may be considered tumor-initiating cells that ultimately progress to skin neoplasm.[28] As a further confirmation at the transcriptional level, we performed qRT-PCR assays to examine mRNA expression of *CCND1*(encoding the protein Cyclin D1) and *MYC* (encoding the protein c-MYC). Compared to healthy skin, up-regulation of eIF4 proteins in HS skin coincided with the significantly increased mRNA for *CCND1* and *MYC* (Figure 6D). Confocal microscopy confirmed the presence of nuclear Cyclin D1/CDK4 complex in HS epithelial cells (Figure 6E). We also observed that PCNA, a hallmark of cell proliferation, was up-regulated and co-localized with c-MYC in the nuclei of hyperproliferative epidermal cells within HS lesions but not in healthy skin (Figure 6F).

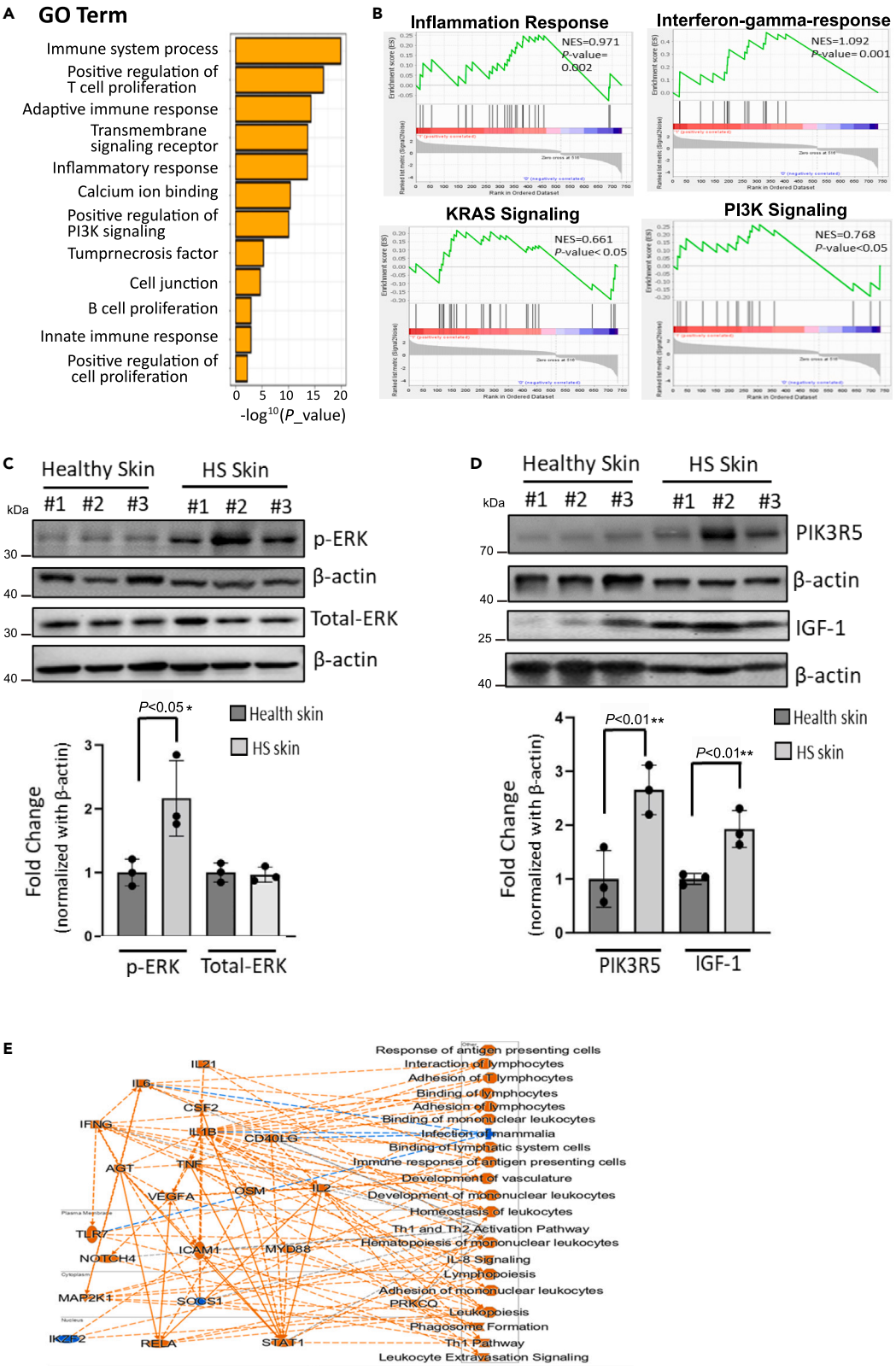
A
GO Term
Immune system process
Positive regulation of T cell proliferation
Adaptive immune response
Transmembrane signaling receptor
Inflammatory response
Calcium ion binding
Positive regulation of PI3K signaling
Tumprnecrosis factor
Cell junction
B cell proliferation
Innate immune response
Positive regulation of cell proliferation
0 5 10 15 20
-log10(P_value)
B
Inflammation Response
NES=0.971
P-value= 0.002
Interferon-gamma-response
NES=1.092
P-value= 0.001
KRAS Signaling
NES=0.661
P-value< 0.05
PI3K Signaling
NES=0.768
P-value<0.05
C
Healthy Skin
HS Skin
kDa
#1 #2 #3 #1 #2 #3
30
p-ERK
40
β-actin
30
Total-ERK
40
β-actin
P<0.05 *
Health skin
HS skin
Fold Change
(normalized with β-actin)
p-ERK
Total-ERK
D
Healthy Skin
HS Skin
kDa
#1 #2 #3 #1 #2 #3
70
PIK3R5
40
β-actin
25
IGF-1
40
β-actin
P<0.01**
P<0.01**
Health skin
HS skin
Fold Change
(normalized with β-actin)
PIK3R5
IGF-1
E
IL21
IL6
CSF2
IFNG
IL1B
CD40LG
AGT
TNF
VEGFA
OSM
IL2
TLR7
NOTCH4
ICAM1
MYD88
MAP2K1
SOCS1
IKZF2
RELA
STAT1
Response of antigen presenting cells
Interaction of lymphocytes
Adhesion of T lymphocytes
Binding of lymphocytes
Adhesion of lymphocytes
Binding of mononuclear leukocytes
Infection of mammalia
Binding of lymphatic system cells
Immune response of antigen presenting cells
Development of vasculature
Development of mononuclear leukocytes
Homeostasis of leukocytes
Th1 and Th2 Activation Pathway
Hematopoiesis of mononuclear leukocytes
IL-8 Signaling
Lymphopoiesis
Adhesion of mononuclear leukocytes
PRKCQ
Leukopoiesis
Phagosome Formation
Th1 Pathway
Leukocyte Extravasation Signaling

Figure 4. GO analysis of eIF4F-associated DEGs in HS skin

(A) GO enrichment analysis showing the top 12 ranked biological functions for eIF4F-related DEGs in HS skin. The Y axis represents the p-value (log-scaled).

(B) GSEA tool was employed to analyze hallmark signals enriched in HS skin.

(C) *Left*, Western blot analysis of the *p*-ERK and ERK expression in HS skin compared to those in healthy skin. *Right*, Histogram showing densitometry analysis of band intensity and presented in fold change (n = 3 individual samples per group). Data are represented as mean ± SEM. p-values based on unpaired two-tailed Student's *t* test. *$p < 0.05$.

(D) *Left*, Western blot analysis of the protein expression for two indicated PI3K targets in healthy and HS skin. *Right*, Histogram showing densitometry analysis of band intensity and presented in fold change (n = 3 individual samples per group). Data are represented as mean ± SEM. p-values based on unpaired two-tailed Student's *t* test. **$p < 0.01$.

(E) IPA analysis for DEGs generated from Figure 4C. Each individual module or line (orange and blue) indicates the increasing and decreasing state.

See also Figure S2.

eIF4F and nuclear Cyclin D1/c-MYC in the pathogenesis of HS-associated cSCC

To assess the *in vivo* significance of our findings in the context of cSCC, we examined the tissue expression of eIF4F complex proteins in cancer specimens derived from HS patients. These neoplasms were histologically confirmed as keratoacanthoma-type cSCCs (KA-type cSCCs) through H&E staining (Figure 7A), by a dermatologist who is also a coauthor in this manuscript. The high expression of eIF4F proteins correlated with poor differentiation and dermal invasion of cSCC cells. Like our earlier observations, weak IF staining of eIF4F proteins was confined mainly to the epidermal layer of healthy skin of race- and sex-matched cohorts (Figures 7B and S4A). In contrast, the high expression of eIF4E and eIF4A1 as well as moderate expression of eIF4G were distributed throughout tumor lesions (Figure S4B). The expression of these proteins was more profound in the hyperproliferative compartment expanding to the hypodermal regions of the tumor as compared to the more differentiated area of the tumor near the crater of KA (Figure S4). IF studies ascertained the co-localization of the eIF4F protein complex (Figure 7C).

After demonstrating the expression of the eIF4F complex in cSCC is contiguous with that of the hyperproliferative epidermal compartment of HS skin, we examined the expression of its translational targets, Cyclin D1 and c-MYC. We also included a Cyclin D1 kinase partner CDK4 in this staining. In confocal IF images, nuclear Cyclin D1 and c-MYC proteins were prominently present in the outer layers of tumor cells in contrast to their expression in the basal layers of the healthy epidermis (Figures 8A and S5A). Thus, we identified the co-localization of both the eIF4F complex and their translational target oncoproteins in the HS-cSCC skin. These observations are highly significant in defining the role of c-MYC alone in creating highly differentiated epithelial cells of the crater filled with keratins, whereas Cyclin D1 and c-MYC caused hyperproliferation and dermal invasion of KA-type sSCCs (Figures 8B, 8C and S5B).

DISCUSSION

HS is a chronic and recurrent inflammatory skin disease with poorly described underlying molecular mechanisms. Intriguingly, some HS patients develop invasive keratoacanthoma-type squamous cell carcinoma. In this article, we show that 5′-cap-dependent protein translation regulatory complex eIF4F (eIF4E/4G/4A1) is involved in the pathogenesis of HS and regulates follicular hyperproliferation, the key characteristics of this disease. We demonstrate that elevated expression of proteins of the eIF4F complex is contiguous to HS lesion-associated cSCC regulating hyperproliferation response. This is consistent with our recent demonstration of the role of the eIF4F complex in the pathogenesis of UVB-induced human and murine cSCC. We also demonstrate that downstream targets of eIF4F, Cyclin D1, and c-MYC may be involved in the molecular pathogenesis of HS skin-associated invasive KA. In this regard, the spatial localization of these target proteins is unique and provides critical roles in KA pathogenesis. Although nuclear c-MYC drives differentiation of HS epithelial cells leading to the formation of the keratin-filled crater of KA, nuclear co-localization of c-MYC and Cyclin D1 provides oncogenic transformation of these epithelial cells into invasive SCC. Consistently, eIF4F complex-activated RAS and PI3K onco-signaling networks are highly enriched in the HS transcriptome and lead to hyperphosphorylation-dependent ERK activation, which helps in maintaining invasive KA phenotype. Thus, the spatial localization of nuclear Cyclin D1 and c-MYC within the lesional keratinocytes orchestrates molecular pathogenesis of invasive keratoacanthoma associated with HS.

Approximately 1–3.2% of HS patients develop sSCC.[10] In familial HS, loss-of-function mutations have been reported in genes of the γ-secretase complex, including *NCSTN*, *PSEN1*, *PSENEN*, and *PSTPIP1*.[29,30] *NCSTN* mutants dysregulate keratinocyte proliferation and differentiation via activated Notch and PI3K signals,[31] the latter of which plays a prominent role in the pathogenesis of sSCC.[32,33] *NCSTN*, *PSEN1*, and *PSENEN*, mutations have also been reported in sporadic HS from different cohorts of patients (for

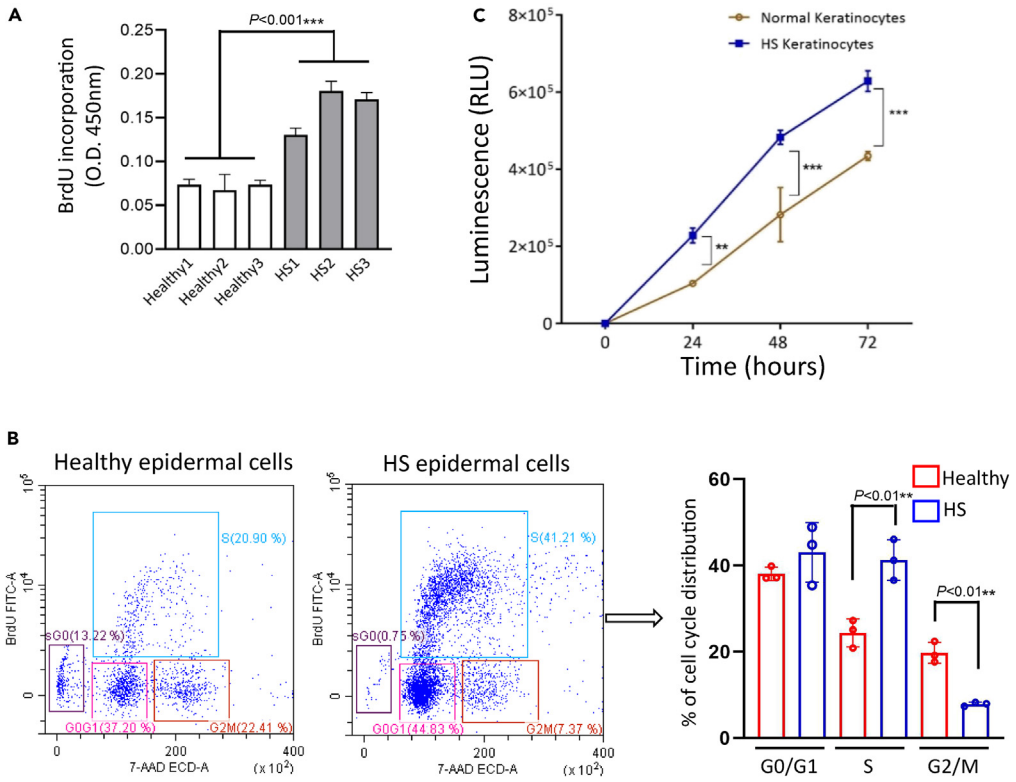

Figure 5. Enhanced cell proliferation in HS epidermis

(A) BrdU incorporation was assessed in epidermal cells obtained from healthy and HS skin (n = 3 individual samples, respectively). Data are represented as mean ± SEM. p-values based on unpaired two-tailed Student's *t* test. ***p < 0.001.

(B) Cell cycle distribution was measured by BrdU-based flow cytometry detection. Fresh epidermal cells were obtained from healthy or HS skin (n = 3 individual samples, respectively). The percentage of the cell numbers in each phase was calculated in three independent experiments. Data are represented as mean ± SEM. p-values based on unpaired two-tailed Student's *t* test. **p < 0.01.

(C) Healthy and HS-derived keratinocytes were seeded in triplicate into 96-well plates. The number of viable cells was measured over time using the CellTiter-Glo luminescent cell viability assay kit (n = 3 individual samples per group). Data are represented as mean ± SEM. p-values based on unpaired two-tailed Student's *t* test. **p < 0.01, ***p < 0.001.

example, Caucasian, European, and Asian), and the incidence rates are up to 3.2%.[34–37] We also found a positive correlation between eIF4F-related induction of the PI3K pathway and HS lesions (Figures 4A, 4D and S2B), establishing the importance of this pathway in HS pathogenesis.

Translation control employed for protein synthesis in cells is tissue context-dependent and provides an energy-efficient cell proliferation strategy. It also regulates mRNA metabolism, a cumbersome and multistep process that includes transcription, alternative splicing, and the export of mRNA to the cytoplasm.[38] The enhanced abundance of eIF4F in the cytoplasm of both epidermal and dermal cells in HS skin biopsies (Figure 1) suggests the aberrant translation initiation control and protein synthesis program.[39] In this study, increased eIF4E/eIF4A1/eIF4G expression associated with the enhanced survival and accelerated proliferation found in SCCs[40,41] was also observed in invasive KA but was contiguous to HS skin, suggesting that these SCCs originate from HS skin epithelial cells. However, nuclear expression of oncogenic Cyclin D1 and c-MYC in cSCC cells points to their role as cancer drivers and confirms their distinct participation in the molecular pathogenesis of invasive KA (Figure 8B). Consistent with the earlier demonstration of their role in human epidermal tumorigenesis,[42] our observation that CDK4 is co-overexpressed with Cyclin D1 in these cells (Figure 6E), provides a mechanism underlying the malignant progression of HS epithelial cells. Of note, eIF4F components show their distinct distribution within the tumor areas expanding into the dermis of HS lesions. We found slightly weaker

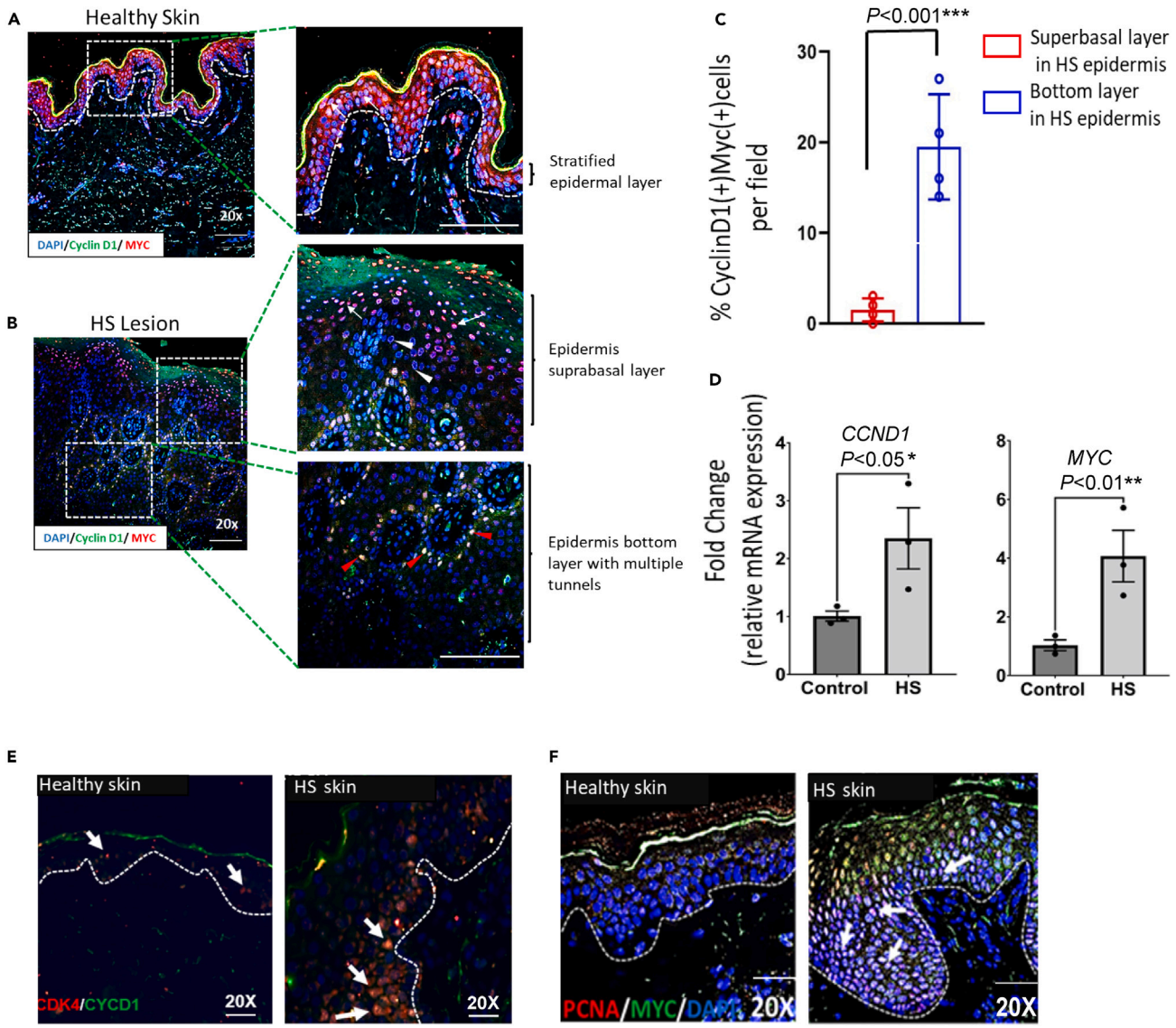

Figure 6. Overexpression patterns of Cyclin D1 and c-MYC in HS epidermis

(A) Representative confocal images of IF staining for Cyclin D1 (green), c-MYC (red), and DAPI (blue), in the healthy human stratified epidermal layer (left panel). White arrow of the magnified area (right panel) indicating that the protein of Cyclin D1 is localized in the cellular cytoplasm of epidermal cells. Scale bar = 100 μm. The experiment was performed on 8 individual samples and had similar results.

(B) IF staining of Cyclin D1 (green), c-MYC (red), and DAPI (blue), in HS lesions (left panel). The magnified area (right upper panel) shows that Cyclin D1 is localized in the cellular cytoplasm (white arrow) while c-MYC is specifically expressed in cellular nuclei (white arrowhead) in the HS suprabasal epidermis. The magnified area (right bottom panel) shows the nuclei co-localization of Cyclin D1 and c-MYC in some peripheral cells forming tunnels in the HS epidermis (red arrow). Scale bar = 100 μm. The experiment was performed on 8 individual samples and had similar results.

(C) Bar graphs showing the quantitative analysis of Cyclin D(+)/MYC(+) cells from (B) (n = 4 random areas per sample). Data are represented as mean ± SEM. p-values based on unpaired two-tailed Student's *t* test. ***p < 0.001.

(D) Data from TaqMan qRT-PCR validate the enhanced expression of *CCND1* and *MYC* mRNA in HS skin (n = 3 samples per group). The Y axis represents the fold change. GAPDH expression was used for normalization. Data are represented as mean ± SEM. p-values based on unpaired two-tailed Student's *t* test. *p < 0.05, **p < 0.01.

(E and F) Confocal images demonstrating the co-localization of Cyclin D1/CDK4 and PCNA/MYC in the epidermis of healthy and HS skin. The white arrow showed the nuclear co-localization of indicated proteins in healthy and HS epidermis, respectively. White dot line indicates the junction of epidermal and dermal compartments. Scale bar = 100 μm. The experiment was performed on 8 individuals for healthy and HS skin, respectively, and had similar results. See also Figure S3.

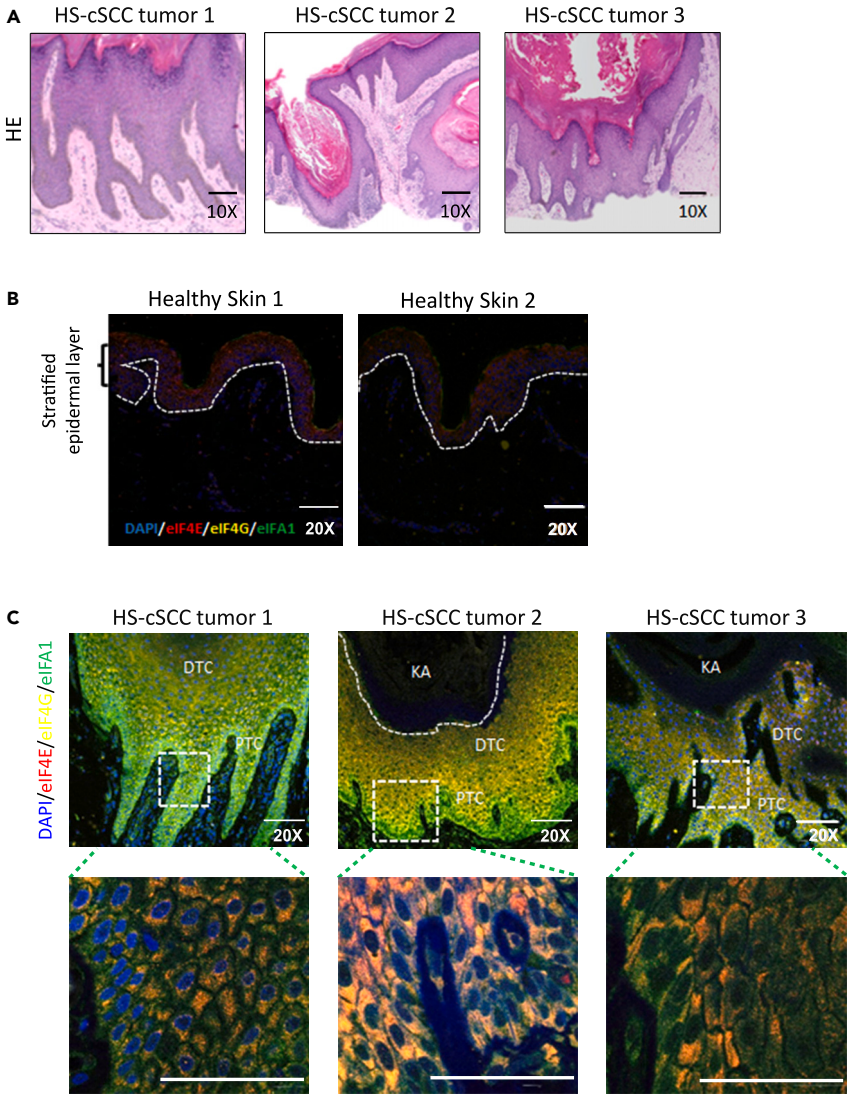

Figure 7. High-resolution confocal images of eIF4E/eIF4A1/eIF4G in human HS-associated cSCC

(A) Representative H&E staining of HS-cSCC skin sections. Scale bar = 50 μm.

(B) Representative IF staining shows the expression of eIF4E (red), eIF4G (yellow), and eIF4A1 (green), along with DAPI (blue), in healthy skin. The white dot line indicates the junction of epidermal and dermal compartments. Scale bar = 100 μm.

(C) Upper, representative images showing the enhanced expression of eIF4E (red), eIF4G (yellow), eIF4A1 (green), and DAPI (blue) in cSCC samples from three HS patients. The white dot line indicates the junction of keratin and tumor cells. Scale bar = 100 μm. Bottom, zoom the area of images from the respective middle panel. White dot box indicating the region with the overlapping protein expression for eIF4E/eIF4A1/eIF4G.

See also Figure S4.

signals for eIF4G and eIF4A1 when compared with the expression and distribution of eIF4E (Figure 2C, i-iii). These data suggest eIF4F complex components have additional unique roles in delineating the highly heterogeneous cell populations, which is consistent with the known pathogenesis of most cancers.[43] It is important to mention that c-MYC plays distinct roles in normal skin. Its activation in transit-amplifying keratinocytes causes a progressive reduction in cell growth by stimulating terminal differentiation,[44] while in stem cells, c-MYC drives the generation of transit-amplifying keratinocytes.[44] Our data indicate that these unique properties of c-MYC orchestrate the pathogenesis of invasive KA. Although enhanced expression of c-MYC alone leads to the differentiation of HS-associated epithelial cells, a crucial signal required for the formation of the keratin-filled crater of the KA, the combined nuclear expression of c-MYC and Cyclin D1/CDK4 drives invasive squamous lesions invading into the dermis (Figure 8B).

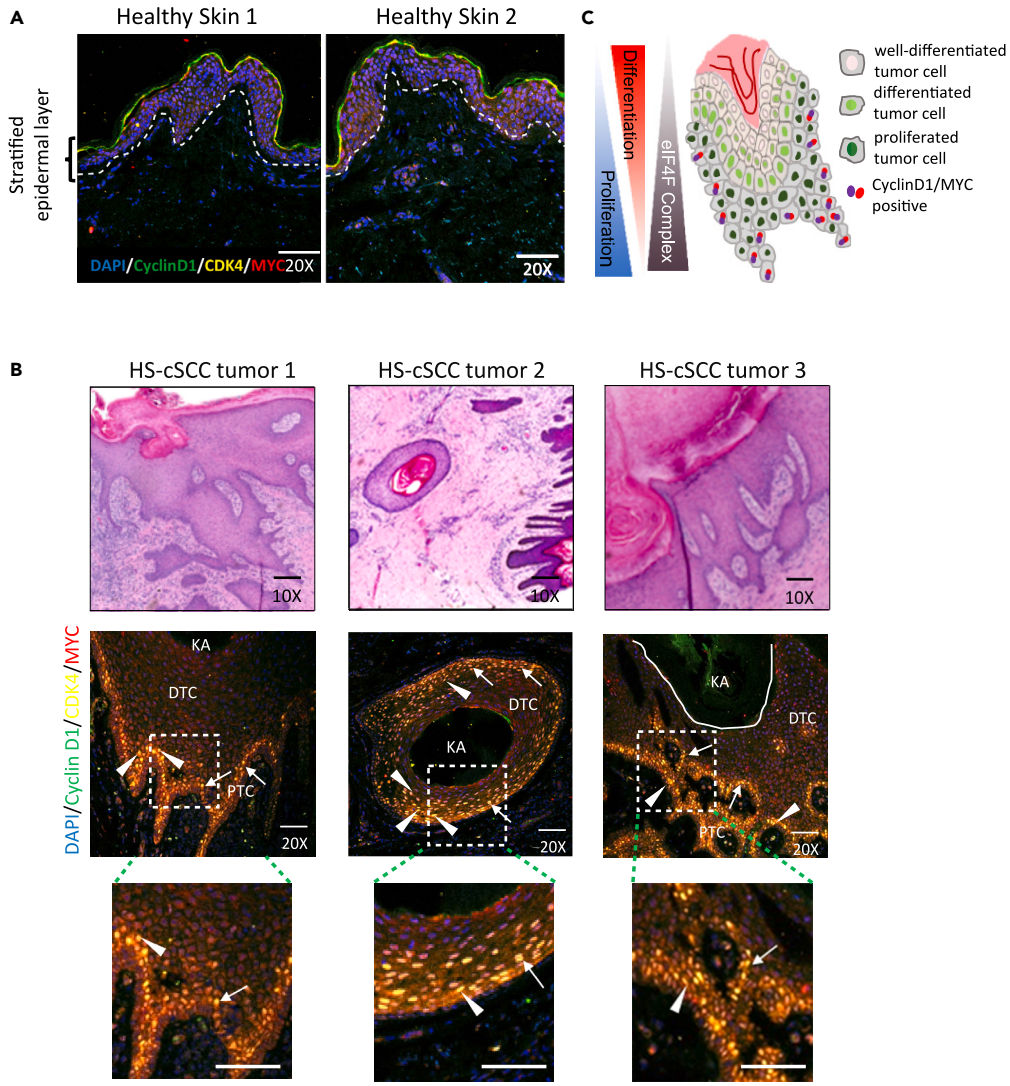

Figure 8. Overexpression patterns of Cyclin D1 and c-Myc as well as CDK4 in HS-cSCC specimen

(A) Representative IF staining images showing the protein expression of Cyclin D1 (green), CDK4 (yellow), c-Myc (red), and DAPI (blue), in healthy skin (n = 2 individuals). White dot line indicates the junction of epidermal and dermal compartments. Scale bar = 100 μm.

(B) *Upper*, representative H&E staining of HS-cSCC skin sections from three HS patients. *Middle*, representative confocal IF staining of Cyclin D1 (green), CDK4 (yellow), c-MYC (red), and DAPI (blue) in cSCC samples. White arrowhead showing the co-localization of CyclinD1-CDK4 inside nuclei; white arrow showing merged signaling for Cyclin D1 and c-Myc in nuclei. *Bottom*, zoom the area of images from the respective middle panel. Scale bar = 100 μm.

(C) Cartoon for the distribution of Cyclin D1 and c-MYC in HS-cSCC tumor.

See also Figure S5.

As reported in the skin of HS patients, keratinocytes, dermal fibroblast, and immune cells, including skin resident DCs, LCs, and melanocytes, secrete a wide spectrum of immune-related clastogenic molecules (e.g., cytokines, chemokines, and growth factors) to create a robust inflammatory microenvironment conducive to the pathogenesis of SCC.[45] Enrichment of eIF4F-associated inflammatory pathways such as IFN-γ, TNF, and IL6 signaling pathways (Figure 4E), promotes immune cell infiltration and survival of tumor cells enabling them for metastasis.[46]

Previous studies indicated that deficiency of the Notch pathway in familial HS regulates the pathogenesis by crosstalk with PI3K/AKT pathway[47] or EGFR signaling.[48] However, the pathways which orchestrate the

complex non-familial HS pathogenesis remain undefined. This is the first report (to the best of our knowledge) showing that the RAS/MEK/ERK oncogenic signaling pathway in collaboration with protein translation complex eIF4F mediates HS pathogenesis and associated invasive KA (Figure 7C). It is known that the RAS/MEK/ERK pathway plays a critical role in cell proliferation and cell survival, and its aberrant activation causes cutaneous tumorigenesis.[49] Importantly, we demonstrate augmented RAS signaling in HS skin (Figure 4C). In addition, we also identified numerous RAS target genes (e.g., *WNT5A*, *IL6*, *IL1B*, *PDGFRB*, *NOX4*, *IGF1*, *CARD9*, *CCR1*, and *EPHA10*) involved in signal transduction, cytokine signaling, and cancer development (Figure S2A). Thus, the eIF4F complex is an important context-dependent mediator for both hyperproliferation and transformation of HS epithelial cells. In the future, identifying this aberrant profile of signals in various pathogenic cell types present in late-stage HS may add a new dimension to the molecular pathogenesis of HS-cSCC and help prevent the development of lethal cSCC in HS patients. Phosphorylation-dependent activation of ERK in HS lesions (Figure 4C), suggests a novel therapeutic target for treating HS and its associated invasive KA, because it is known that blocking ERK may lead to regression of invasive KA.[50]

In summary, our data provide a novel potential mechanism by which 5′-cap translation initiation factor proteins, eIF4E, eIF4A1, and eIF4G, and associated target oncogenic proteins Cyclin D1 and c-MYC, orchestrate follicular hyperproliferation associated sinus tract formation as well as tissue microenvironment conducive to malignant transformation and KA-cSCC development in Hurley stage II/III patients. We also propose that ERK may serve as a potential therapeutic target for suppressing the pathogenesis of these lesions. Importantly, FDA-approved ERK inhibitors are available as antineoplastic drugs.

Limitations of the study

There are no mouse models of HS available that can recapitulate the human disease faithfully. The sample size of HS-associated KA is rather small in this study. Small molecule-based pathway inhibition studies will be helpful for which novel disease models are required in future studies.

STAR★METHODS

Detailed methods are provided in the online version of this paper and include the following:

- KEY RESOURCES TABLE
- RESOURCE AVAILABILITY
  - Lead contact
  - Materials availability
  - Data and code availability
- EXPERIMENTAL MODEL AND STUDY PARTICIPANT DETAILS
  - Primary epidermal cells
  - Human subjects
- METHOD DETAILS
  - Immunohistochemistry (IHC)
  - Confocal immunofluorescence (IF) staining
  - Bromodeoxyuridine (BrdU) cell proliferation assay
  - Cell cycle measurement
  - Cell viability assay
  - qRT-PCR
  - Western-blot assay
  - RNA-seq analysis
  - Gene set enrichment analysis (GSEA) and ingenuity pathway analysis (IPA)
- QUANTIFICATION AND STATISTICAL ANALYSIS

SUPPLEMENTAL INFORMATION

Supplemental information can be found online at https://doi.org/10.1016/j.isci.2023.106896.

ACKNOWLEDGMENTS

This work is in part supported by NIH grant RO1 ES026219, R01CA276683, and P01CA210946, and by intramural UAB funds to M.A. and other authors (C.A.E., and V.A.) of this manuscript. We are grateful to Leslie M. Roop for the final editing of the manuscript.

AUTHOR CONTRIBUTIONS

Conceptualization: L.J. and M.A. Methodology: L.J., M.P.K., Y.C., J.K., J.C., M.B.L., A.O., R.S., and V.A. Investigation: L.J., M.P.K., Y.C., J.K., Y.G., Z.W., and R.S. Visualization: L.J. and Y.C. Experimental advice: S.M.M., J.S.D., and C.R. Clinical design: P.P., T.M., C.E., B.E.E, and C.A.E. Supervision: M.A. Writing–original draft: L.J and M.A. Writing–review and editing: L.J. and M.A.

DECLARATION OF INTERESTS

Authors of this manuscript have no conflict of interest between them or anybody else regarding the scientific contents, financial matters, or otherwise.

Received: April 3, 2023
Revised: April 23, 2023
Accepted: May 12, 2023
Published: May 19, 2023

REFERENCES

1. Jemec, G.B.E. (2012). Clinical practice. Hidradenitis suppurativa. N. Engl. J. Med. *366*, 158–164. https://doi.org/10.1056/NEJMcp1014163.

2. Matusiak, Ł., Bieniek, A., and Szepietowski, J.C. (2010). Hidradenitis suppurativa markedly decreases quality of life and professional activity. J. Am. Acad. Dermatol. *62*, 706–708. https://doi.org/10.1016/j.jaad.2009.09.021.

3. Jemec, G.B., Heidenheim, M., and Nielsen, N.H. (1996). The prevalence of hidradenitis suppurativa and its potential precursor lesions. J. Am. Acad. Dermatol. *35*, 191–194. https://doi.org/10.1016/s0190-9622(96)90321-7.

4. Saunte, D.M.L., and Jemec, G.B.E. (2017). Hidradenitis suppurativa: advances in diagnosis and treatment. JAMA *318*, 2019–2032. https://doi.org/10.1001/jama.2017.16691.

5. Sabat, R., Jemec, G.B.E., Matusiak, Ł., Kimball, A.B., Prens, E., and Wolk, K. (2020). Hidradenitis suppurativa. Nat. Rev. Dis. Prim. *6*, 18. https://doi.org/10.1038/s41572-020-0149-1.

6. Hurley, H., Roenigk, R., and Roenigk, H. (1989). Dermatologic Surgery, Principles and Practice (Marcel).

7. Alavi, A. (2015). Hidradenitis suppurativa: demystifying a chronic and debilitating disease. J. Am. Acad. Dermatol. *73*, S1–S2. https://doi.org/10.1016/j.jaad.2015.08.061.

8. Gudjonsson, J.E., Tsoi, L.C., Ma, F., Billi, A.C., van Straalen, K.R., Vossen, A., van der Zee, H.H., Harms, P.W., Wasikowski, R., Yee, C.M., et al. (2020). Contribution of plasma cells and B cells to hidradenitis suppurativa pathogenesis. JCI Insight *5*, e139930. https://doi.org/10.1172/jci.insight.139930.

9. Yon, J.R., Son, J.D., Fredericks, C., Morton, M., Kingsley, S., Gupta, S., Poulakidas, S., and Bokhari, F. (2017). Marjolin's ulcer in chronic hidradenitis suppurativa: a rare complication of an often neglected disease. J. Burn Care Res. *38*, 121–124. https://doi.org/10.1097/BCR.0000000000000399.

10. Roy, C.F., Roy, S.F., Ghazawi, F.M., Patocskai, E., Bélisle, A., and Dépeault, A. (2019). Cutaneous squamous cell carcinoma arising in hidradenitis suppurativa: a case report. SAGE Open Med. Case Rep. *7*. 2050313X19847359. https://doi.org/10.1177/2050313X19847359.

11. Juviler, P.G., Patel, A.P., and Qi, Y. (2019). Infiltrative squamous cell carcinoma in hidradenitis suppurativa: a case report for early surgical intervention. Int. J. Surg. Case Rep. *55*, 50–53. https://doi.org/10.1016/j.ijscr.2019.01.006.

12. Constantinou, C., Widom, K., Desantis, J., and Obmann, M. (2008). Hidradenitis suppurativa complicated by squamous cell carcinoma. Am. Surg. *74*, 1177–1181.

13. Hua, V.J., Kilgour, J.M., Cho, H.G., Li, S., and Sarin, K.Y. (2021). Characterization of comorbidity heterogeneity among 13,667 patients with hidradenitis suppurativa. JCI Insight *6*, e151872. https://doi.org/10.1172/jci.insight.151872.

14. Buszczak, M., Signer, R.A.J., and Morrison, S.J. (2014). Cellular differences in protein synthesis regulate tissue homeostasis. Cell *159*, 242–251. https://doi.org/10.1016/j.cell.2014.09.016.

15. Kumar, P., Hellen, C.U.T., and Pestova, T.V. (2016). Toward the mechanism of eIF4F-mediated ribosomal attachment to mammalian capped mRNAs. Genes Dev. *30*, 1573–1588. https://doi.org/10.1101/gad.282418.116.

16. Kosciuczuk, E.M., Saleiro, D., and Platanias, L.C. (2017). Dual targeting of eIF4E by blocking MNK and mTOR pathways in leukemia. Cytokine *89*, 116–121. https://doi.org/10.1016/j.cyto.2016.01.024.

17. Frosi, Y., Usher, R., Lian, D.T.G., Lane, D.P., and Brown, C.J. (2019). Monitoring flux in signalling pathways through measurements of 4EBP1-mediated eIF4F complex assembly. BMC Biol. *17*, 40. https://doi.org/10.1186/s12915-019-0658-0.

18. Pelletier, J., Graff, J., Ruggero, D., and Sonenberg, N. (2015). Targeting the eIF4F translation initiation complex: a critical nexus for cancer development. Cancer Res. *75*, 250–263. https://doi.org/10.1158/0008-5472.CAN-14-2789.

19. Srivastava, R.K., Khan, J., Arumugam, A., Muzaffar, S., Guroji, P., Gorbatyuk, M.S., Elmets, C.A., Slominski, A.T., Mukhtar, M.S., and Athar, M. (2021). 5′-Cap−Dependent translation as a potent therapeutic target for lethal human squamous cell carcinoma. J. Invest. Dermatol. *141*, 742–753.e10. https://doi.org/10.1016/j.jid.2020.08.021.

20. De Benedetti, A., and Graff, J.R. (2004). eIF-4E expression and its role in malignancies and metastases. Oncogene *23*, 3189–3199. https://doi.org/10.1038/sj.onc.1207545.

21. Boussemart, L., Malka-Mahieu, H., Girault, I., Allard, D., Hemmingsson, O., Tomasic, G., Thomas, M., Basmadjian, C., Ribeiro, N., Thuaud, F., et al. (2014). eIF4F is a nexus of resistance to anti-BRAF and anti-MEK cancer therapies. Nature *513*, 105–109. https://doi.org/10.1038/nature13572.

22. Robichaud, N., Hsu, B.E., Istomine, R., Alvarez, F., Blagih, J., Ma, E.H., Morales, S.V., Dai, D.L., Li, G., Souleimanova, M., et al. (2018). Translational control in the tumor microenvironment promotes lung metastasis: phosphorylation of eIF4E in neutrophils. Proc. Natl. Acad. Sci. USA *115*, E2202–E2209. https://doi.org/10.1073/pnas.1717439115.

23. Cerezo, M., Guemiri, R., Druillennec, S., Girault, I., Malka-Mahieu, H., Shen, S., Allard, D., Martineau, S., Welsch, C., Agoussi, S., et al. (2018). Translational control of tumor immune escape via the eIF4F-STAT1-PD-L1 axis in melanoma. Nat. Med. *24*, 1877–1886. https://doi.org/10.1038/s41591-018-0217-1.

24. Osborne, M.J., and Borden, K.L.B. (2015). The eukaryotic translation initiation factor eIF4E in the nucleus: taking the road less traveled. Immunol. Rev. *263*, 210–223. https://doi.org/10.1111/imr.12240.

25. Lowe, M.M., Naik, H.B., Clancy, S., Pauli, M., Smith, K.M., Bi, Y., Dunstan, R., Gudjonsson, J.E., Paul, M., Harris, H., et al. (2020). Immunopathogenesis of hidradenitis

suppurativa and response to anti-TNF-α therapy. JCI Insight *5*, e139932. https://doi.org/10.1172/jci.insight.139932.

26. Chan, K., Robert, F., Oertlin, C., Kapeller-Libermann, D., Avizonis, D., Gutierrez, J., Handly- Santana, A., Doubrovin, M., Park, J., Schoepfer, C., et al. (2019). eIF4A supports an oncogenic translation program in pancreatic ductal adenocarcinoma. Nat. Commun. *10*, 5151. https://doi.org/10.1038/s41467-019-13086-5.

27. Fernández-Hernández, R., Rafel, M., Fusté, N.P., Aguayo, R.S., Casanova, J.M., Egea, J., Ferrezuelo, F., and Garí, E. (2013). Cyclin D1 localizes in the cytoplasm of keratinocytes during skin differentiation and regulates cell-matrix adhesion. Cell Cycle *12*, 2510–2517. https://doi.org/10.4161/cc.25590.

28. Kim, J.K., and Diehl, J.A. (2009). Nuclear cyclin D1: an oncogenic driver in human cancer. J. Cell. Physiol. *220*, 292–296. https://doi.org/10.1002/jcp.21791.

29. Liu, M., Davis, J.W., Idler, K.B., Mostafa, N.M., Okun, M.M., and Waring, J.F. (2016). Genetic analysis of NCSTN for potential association with hidradenitis suppurativa in familial and nonfamilial patients. Br. J. Dermatol. *175*, 414–416. https://doi.org/10.1111/bjd.14482.

30. Ingram, J.R., Wood, M., John, B., Butler, R., and Anstey, A.V. (2013). Absence of pathogenic gamma-secretase mutations in a South Wales cohort of familial and sporadic hidradenitis suppurativa (acne inversa). Br. J. Dermatol. *168*, 874–876. https://doi.org/10.1111/bjd.12048.

31. Xiao, X., He, Y., Li, C., Zhang, X., Xu, H., and Wang, B. (2016). Nicastrin mutations in familial acne inversa impact keratinocyte proliferation and differentiation through the Notch and phosphoinositide 3-kinase/AKT signalling pathways. Br. J. Dermatol. *174*, 522–532. https://doi.org/10.1111/bjd.14223.

32. Liu, P., Cheng, H., Roberts, T.M., and Zhao, J.J. (2009). Targeting the phosphoinositide 3-kinase pathway in cancer. Nat. Rev. Drug Discov. *8*, 627–644. https://doi.org/10.1038/nrd2926.

33. Cai, Y., Dodhia, S., and Su, G.H. (2017). Dysregulations in the PI3K pathway and targeted therapies for head and neck squamous cell carcinoma. Oncotarget *8*, 22203–22217. https://doi.org/10.18632/oncotarget.14729.

34. Vural, S., Baumgartner, M., Lichtner, P., Eckstein, G., Hariry, H., Chen, W.C., Ruzicka, T., Melnik, B., Plewig, G., Wagner, M., and Giehl, K.A. (2021). Investigation of gamma secretase gene complex mutations in German population with Hidradenitis suppurativa designate a complex polygenic heritage. J. Eur. Acad. Dermatol. Venereol. *35*, 1386–1392. https://doi.org/10.1111/jdv.17163.

35. Duchatelet, S., Miskinyte, S., Delage, M., Ungeheuer, M.N., Lam, T., Benhadou, F., Del Marmol, V., Vossen, A., Prens, E.P., Cogrel, O., et al. (2020). Low prevalence of GSC gene mutations in a large cohort of predominantly caucasian patients with hidradenitis suppurativa. J. Invest. Dermatol. *140*, 2085–2088.e14. https://doi.org/10.1016/j.jid.2019.10.025.

36. Ralser, D.J., Basmanav, F.B.Ü., Tafazzoli, A., Wititsuwannakul, J., Delker, S., Danda, S., Thiele, H., Wolf, S., Busch, M., Pulimood, S.A., et al. (2017). Mutations in gamma-secretase subunit-encoding PSENEN underlie Dowling-Degos disease associated with acne inversa. J. Clin. Invest. *127*, 1485–1490. https://doi.org/10.1172/JCI90667.

37. Nomura, T. (2020). Hidradenitis suppurativa as a potential subtype of autoinflammatory keratinization disease. Front. Immunol. *11*, 847. https://doi.org/10.3389/fimmu.2020.00847.

38. Carmody, S.R., and Wente, S.R. (2009). mRNA nuclear export at a glance. J. Cell Sci. *122*, 1933–1937. https://doi.org/10.1242/jcs.041236.

39. Sendoel, A., Dunn, J.G., Rodriguez, E.H., Naik, S., Gomez, N.C., Hurwitz, B., Levorse, J., Dill, B.D., Schramek, D., Molina, H., et al. (2017). Translation from unconventional 5′ start sites drives tumour initiation. Nature *541*, 494–499. https://doi.org/10.1038/nature21036.

40. Bauer, C., Brass, N., Diesinger, I., Kayser, K., Grässer, F.A., and Meese, E. (2002). Overexpression of the eukaryotic translation initiation factor 4G (eIF4G-1) in squamous cell lung carcinoma. Int. J. Cancer *98*, 181–185. https://doi.org/10.1002/ijc.10180.

41. Chakravarti, N., Kadara, H., Yoon, D.J., Shay, J.W., Myers, J.N., Lotan, D., Sonenberg, N., and Lotan, R. (2010). Differential inhibition of protein translation machinery by curcumin in normal, immortalized, and malignant oral epithelial cells. Cancer Prev. Res. *3*, 331–338. https://doi.org/10.1158/1940-6207.CAPR-09-0076.

42. Lazarov, M., Kubo, Y., Cai, T., Dajee, M., Tarutani, M., Lin, Q., Fang, M., Tao, S., Green, C.L., and Khavari, P.A. (2002). CDK4 coexpression with Ras generates malignant human epidermal tumorigenesis. Nat. Med. *8*, 1105–1114. https://doi.org/10.1038/nm779.

43. Smith, R.C.L., Kanellos, G., Vlahov, N., Alexandrou, C., Willis, A.E., Knight, J.R.P., and Sansom, O.J. (2021). Translation initiation in cancer at a glance. J. Cell Sci. *134*, jcs248476. https://doi.org/10.1242/jcs.248476.

44. Gandarillas, A., and Watt, F.M. (1997). c-Myc promotes differentiation of human epidermal stem cells. Genes Dev. *11*, 2869–2882. https://doi.org/10.1101/gad.11.21.2869.

45. Neagu, M., Constantin, C., Caruntu, C., Dumitru, C., Surcel, M., and Zurac, S. (2019). Inflammation: a key process in skin tumorigenesis. Oncol. Lett. *17*, 4068–4084. https://doi.org/10.3892/ol.2018.9735.

46. Kelly, S.A., Gschmeissner, S., East, N., and Balkwill, F.R. (1991). Enhancement of metastatic potential by gamma-interferon. Cancer Res. *51*, 4020–4027.

47. Hessam, S., Gambichler, T., Skrygan, M., Scholl, L., Sand, M., Meyer, T., Stockfleth, E., and Bechara, F.G. (2021). Increased expression profile of NCSTN, Notch and PI3K/AKT3 in hidradenitis suppurativa. J. Eur. Acad. Dermatol. Venereol. *35*, 203–210. https://doi.org/10.1111/jdv.16962.

48. He, Y., Xu, H., Li, C., Zhang, X., Zhou, P., Xiao, X., Zhang, W., Wu, Y., Zeng, R., and Wang, B. (2019). Nicastrin/miR-30a-3p/RAB31 Axis regulates keratinocyte differentiation by impairing EGFR signaling in familial acne inversa. J. Invest. Dermatol. *139*, 124–134. https://doi.org/10.1016/j.jid.2018.07.020.

49. Pylayeva-Gupta, Y., Grabocka, E., and Bar-Sagi, D. (2011). RAS oncogenes: weaving a tumorigenic web. Nat. Rev. Cancer *11*, 761–774. https://doi.org/10.1038/nrc3106.

50. Su, F., Viros, A., Milagre, C., Trunzer, K., Bollag, G., Spleiss, O., Reis-Filho, J.S., Kong, X., Koya, R.C., Flaherty, K.T., et al. (2012). RAS mutations in cutaneous squamous-cell carcinomas in patients treated with BRAF inhibitors. N. Engl. J. Med. *366*, 207–215. https://doi.org/10.1056/NEJMoa1105358.

51. Goes, H., Virgens, A.R., de Carvalho, G.C., Pietrobon, A.J., Branco, A., Oliveira, L., Fernandes, I.G., Pereira, N.V., Sotto, M.N., Dos Reis, V.M.S., and Sato, M.N. (2020). Proinflammatory and regulatory mechanisms in allergic contact dermatitis caused by methylchloroisothiazolinone and methylisothiazolinone. Exp. Dermatol. *29*, 490–498. https://doi.org/10.1111/exd.14086.

52. Dobin, A., Davis, C.A., Schlesinger, F., Drenkow, J., Zaleski, C., Jha, S., Batut, P., Chaisson, M., and Gingeras, T.R. (2013). STAR: ultrafast universal RNA-seq aligner. Bioinformatics *29*, 15–21. https://doi.org/10.1093/bioinformatics/bts635.

53. Subramanian, A., Tamayo, P., Mootha, V.K., Mukherjee, S., Ebert, B.L., Gillette, M.A., Paulovich, A., Pomeroy, S.L., Golub, T.R., Lander, E.S., and Mesirov, J.P. (2005). Gene set enrichment analysis: a knowledge-based approach for interpreting genome-wide expression profiles. Proc. Natl. Acad. Sci. USA *102*, 15545–15550. https://doi.org/10.1073/pnas.0506580102.

STAR★METHODS

KEY RESOURCES TABLE

REAGENT or RESOURCE	SOURCE	IDENTIFIER
Antibodies		
eIF4E; Rabbit; 1:100 (IF/IHC); 1:1000 (WB)	Novus	Cat# NBP1-48525 RRID:AB-10011190
eIF4A1; Rabbit; 1:200 (IF/IHC); 1:1000 (WB)	Cell Signal	Cat# 2490 RRID:AB-823487
eIF4G; Rabbit; 1:100 (IF/IHC); 1:1000 (WB)	Cell Signal	Cat# 2469 RRID:AB-2096028
Cyclin D1; Rabbit; 1:200 (IF)	Abcam	Cat# ab16663 RRID:AB-443423
MYC; Mouse; 1:200 (IF)	Cell Signal	Cat# 2276 RRID:AB-331783
PCNA; Rabbit; 1:500 (IF)	Abcam	Cat# ab92552 RRID:AB-10561973
CDK4; Rabbit; 1:200 (IF)	Cell Signal	Cat# 12790 RRID:AB-2631166
p-eIF4E; Rabbit; 1:1000 (WB)	Abcam	Cat# ab76256 RRID:AB-1523534
p-ERK; Rabbit; 1:1000 (WB)	Cell Signal	Cat# 4370 RRID:AB-2315112
ERK; Rabbit; 1:1000 (WB)	Cell Signal	Cat# 9102 RRID:AB-330744
PIK3R5; Rabbit; 1:1000 (WB)	Santa Cruz	Cat# sc130230 RRID:AB-2163645
IGF-1; Mouse; 1:1000 (WB)	Santa Cruz	Cat# sc74116 RRID:AB-1124693
β-Actin; Mouse; 1:20,000 (WB)	Sigma-Aldrich	Cat# A3853 RRID:AB-262137
Biological samples		
Normal skin samples	Obtained from healthy subjects with breast or abdominoplasty reduction surgery according to Institutional Review Board-approved protocols	N/A
HS skin samples	Obtained from HS patients according to Institutional Review Board-approved protocols	N/A
Chemicals, peptides, and recombinant proteins		
Dispase-II	Roche	Cat#04942078001
TRIzol reagent	Invitrogen	Cat#15596026
Critical commercial assays		
BrdU cell proliferation ELISA kit	Abcam	Cat#ab126556
FITC BrdU Flow Kit	BD Bioscience	Cat#559619
CellTiter-Glo 2.0 kit	Promega	Cat#G9242
Super-Script III First-Strand Synthesis System	Invitrogen	Cat#18080051

(*Continued on next page*)

Continued

REAGENT or RESOURCE	SOURCE	IDENTIFIER
Fast SYBR® Green Master Mix Real-Time PCR Master Mix	Applied Biosystems	Car#4385612
Bio-Rad DC protein assay kit	Bio-Rad	Cat#5000112
Deposited data		
RNA-sequece data from HS skin	Lowe et al.[25]	GSE155176
RNA-sequence data from eIF4A inhibitor-treated mouse model	Chan et al.[26]	GSE125380
Original western blot images	This paper	https://data.mendeley.com/drafts/bkwxg4r7jx
Experimental models: Cell lines		
Primary keratoncytes derived from normal and HS skin	This paper	N/A
Oligonucleotides		
Human CRABP1 primers	This paper	N/A
Human CD2 primers	This paper	N/A
Human TBX2 primers	This paper	N/A
Human ARHGAP4 primers	This paper	N/A
Human CLEC4D primers	This paper	N/A
Human MYO1G primers	This paper	N/A
Human LEF1 primers	This paper	N/A
Human MYOZ1 primers	This paper	N/A
Human LHX2 primers	This paper	N/A
Human WNT2B primers	This paper	N/A
TaqMan probe for human Cyclin D1	Thermal Fisher	Cat# Hs00765553-m1
TaqMan probe for human c-Myc	Thermal Fisher	Cat# Hs00153408-m1
Software and algorithms		
Bz X analyzer	KEYENCE	https://www.keyence.com/products/microscope/fluorescence-microscope/bz-x700/models/bz-h4a/
OLYMPUS FV31S	OLYMPUS	https://www.olympus-lifescience.com/en/downloads/detail-iframe/?0[downloads][id]=847252002
FlowJo (v10.8)	FLOWJO	https://www.flowjo.com/solutions/flowjo
GraphPad Prism (v9.0)	GraphPad	https://www.graphpad.com/
STAR	Dobin et al.[52]	https://github.com/alexdobin/STAR
Gene Ontology	GENEONTOLOGY	ftp://ftp.geneontology.org/go/gene-associations/gene_association.mgi.gz
GSEA	Subramanian et al.[53]	https://www.gsea-msigdb.org/gsea/index.jsp
IPA	Qiagen	https://digitalinsights.qiagen.com/products-overview/discovery-insights-portfolio/analysis-and-visualization/qiagen-ipa/

RESOURCE AVAILABILITY

Lead contact

Further information and requests for resources or reagents should be directed to and will be fulfilled by the lead contact, Mohammad Athar (mohammadathar@uabmc.edu).

Materials availability

All reagents are available from commercial sources.

Data and code availability

- Original western blot images have been deposited at Mendeley and are publicly available (https://data.mendeley.com/drafts/bkwxg4r7jx). RNA-seq data were obtained from GEO: GSE155176 and GEO: GSE125380 datasets.[25,26] The lead author will share the microscopy data reported in this paper upon reasonable request.
- This paper does not report original codes.
- Any additional information required to reanalyze the data reported in the available from the lead contact upon request.

EXPERIMENTAL MODEL AND STUDY PARTICIPANT DETAILS

Primary epidermal cells

HS and healthy skin tissues were cut into small pieces and digested with 2.5U/ml Dispase-II (Roche, Cat#04942078001) in Hanks' Balanced Salt Solution (HBSS, Corning, Cat#21-022-CM) overnight at 4°C. After digestion, the epidermis was peeled off and minced. The minced epidermis was incubated with 0.05% trypsin-EDTA at 37°C for 40 min for further digestion. The suspension was filtered through a 40 μm cell strainer and spun down at 300 g at 4°C for 5 min. Collected cells were counted at a density of 100,000 per well and seeded on matrigel precoated 6-well plates supplied with KBM-Gold keratinocyte growth medium (Lonza, Cat# 00192060) at 37°C in a humidified chamber with 5% carbon dioxide. We used keratinocytes (2–4 passages) for performing experiments.

Human subjects

The Institutional Review Board of the University of Alabama at Birmingham approved the protocol (IRB-300005214) for obtaining surgically discarded skin tissues from healthy and HS subjects. Surgical excisions from 8 patients with HS (Hurley stage 2 or 3; five Black females, and three Black males; age> 18 years), as well as 8 healthy cohorts from breast or abdominoplasty reduction surgery (five Black females, two Caucasian females, and one Black male; age> 18 years), were collected. The tissue samples were stored at −80°C or fixed in 10% neutral buffered formalin until further study. In addition, a portion of the tissue was used to prepare and culture epithelial cells.

METHOD DETAILS

Immunohistochemistry (IHC)

Excised tissues were fixed in 10% neutral buffered formalin for 24 h at RT and then stored in 70% ethanol. Tissues were embedded in paraffin and cut into 5 μm sections using a microtome (HM 325, Thermo Fisher Scientific). This was followed by staining with hematoxylin and eosin (H&E). Slides were de-paraffinized, rehydrated in a graded series of alcohol, and microwave-treated in a citrate buffer (pH 6.0). For IHC, endogenous peroxidase activity was blocked using 0.3% hydrogen peroxide. After blocking, primary antibodies for anti-eIF4E, anti-eIF4A1, and anti-eIF4G were added to slides, which were incubated overnight at 4°C. On the following day, the corresponding HRP-linked secondary antibody was applied for 45 min at RT, then washed with PBS (3 times, 10 min). DAB solution was used to develop the signal. Sections were visualized under KEYENCE BZ-X710 digital microscope (KEYENCE) and further analyzed with Bz X analyzer software (KEYENCE).

A semi-quantitative analysis was performed to evaluate IHC immunostaining as previously described.[51] Briefly, the epidermal distribution of stained cells was assessed by the ratio of the area of positive cell layers over the total area of cell layers. For dermal analysis, the relative number of cells per square micrometer was determined by manually counting stained cells from eight random fields per sample.

Confocal immunofluorescence (IF) staining

For IF staining, skin sections were de-paraffinized, rehydrated, then incubated in antigen unmasking solution according to the manufacturer's instructions (Vector laboratories). Sections were placed in a blocking buffer containing 5% normal goat serum in PBST (PBS+0.4% Triton X-100) for 1h at 37 °C. Sections were then incubated with primary antibodies against proteins for anti-eIF4E, anti-eIF4A1, anti-eIF4G, anti-Cyclin D1, anti-MYC, anti-PCNA, and anti-CDK4, in blocking solution overnight at 4 °C. Sequential staining was done for visualization of more than one target in a single specimen. After washing (3 times, 10 min each)

with PBST, sections were re-incubated with the indicated Alexa-Fluor–conjugated anti-goat or anti-rabbit secondary antibodies. Sections were fixed in DAPI containing Vectashield antifade mounting medium (H-1200, Vectorlabs). Lastly, sections were visualized under FLUOVIEW FV3000 confocal microscope (Olympus, USA) equipped with FV3000 Galvo scan unit and FV3IS-SW (v2.3.2.169) software.

Bromodeoxyuridine (BrdU) cell proliferation assay

Freshly-isolated epidermal cells were analyzed using a BrdU cell proliferation ELISA kit (ab126556, Abcam). Briefly, isolated cells were seeded into 96-well plates at 4×10^3 cells per well and were maintained at 37°C for 24 h. Then, 20 μL of BrdU was added into the KBM-Gold culture medium, followed by incubation at 37°C for 6 h. After incubation with anti-BrdU antibody and peroxidase-conjugated goat anti-mouse IgG, successively, 100 μL of TMB peroxidase substrate was added, and the mixture was kept at room temperature for 30 min in the dark. The reaction was stopped using a stop solution, and absorbance at a dual wavelength of 450/550 nm was measured by a multi-mode reader (Synergy *Neo*2 Hybrid Multi-mode Reader, BioTek).

Cell cycle measurement

BrdU-based flow cytometry detection was conducted using a FITC BrdU Flow Kit (Cat #, BD Bioscience) according to the manufacturer's instructions. Freshly-isolated epidermal cells were cultured in KBM-Gold culture medium for 24 h before treatment with 10 μM BrdU for 6 h. The cells were fixed and permeabilized with BD Cytofix/Cytoperm Buffer and BD Buffer Plus as well as BD Cytofix/Cytoperm Buffer in sequence. Then, cells were treated with DNase before incubation with an anti-BrdU-FITC antibody followed by 7-AAD. Cell cycle data were collected with a FACS flow cytometer (CytoFLEX S, Beckman Coulter).

Cell viability assay

Skin-derived keratinocytes were trypsinized, counted on a hemocytometer, and seeded on a white background plate at a density of 5,000 per well in triplicate. These cells grew for 7 days at 37°C in a humidified chamber with 5% carbon dioxide. After 0,2,4, and 6 days, a luminescent cell viability assay was conducted using CellTiter-Glo 2.0 kit (Promega, Cat# G9242) according to the manufacturer's instructions. Fluorescence intensity was measured at $485–500nm_{Ex}/520–530nm_{Em}$.

qRT-PCR

Total RNA was extracted with TRIzol reagent (Invitrogen, Cat# 15596026) and reverse-transcribed using the Super-Script III First-Strand Synthesis System (Invitrogen, Cat#18080051) with $Oligo(dT)_{20}$ primers. For gene expression, qPCR was performed with Fast SYBR Green Master Mix Real-Time PCR Master Mix (Applied Biosystems, Cat#4385612) on QuantStudio 12K Flex (Applied Biosystems) machine. The cycling acquisition program was as follows: 95 °C for 20 s, 40 cycles of 95 °C for 3 s, 60 °C for 30 s. Primer information can be seen in Table S2.

Western-blot assay

Protein quantification and western blot analyses were performed as previously described.[19] Briefly, whole-tissue lysates were prepared in RIPA buffer and sonicated. Tissue lysates were then centrifuged at 10,000g for 15 min at 4 °C; the obtained supernatant was used for protein concentration estimation with a Bio-Rad DC protein assay kit (Bio-Rad, CA). Approximately 30–40 μg of protein was loaded into each well of an SDS-PAGE gel, electrophoresed, and transferred onto a polyvinylidene difluoride membrane. Membranes were blocked in 5% milk in Tris-buffered saline-Tween 20 for 1 h and then incubated with primary antibodies for anti-*p*-eIF4E (Ser209), anti-eIF4E, anti-eIF4A1, and anti-eIF4G overnight at 4°C. After three consecutive washes with PBST, membranes were incubated with horseradish peroxidase–conjugated secondary antibodies diluted in 5% milk for 2 h, washed with PBST, and developed using enhanced chemiluminescence detection reagent. For sequential β-Actin antibody re-probing, blots were stripped using Restore Plus Western Blot Stripping Buffer (Pierce Biotechnology) according to the manufacturer's instructions. Band intensity was determined by densitometry and normalized to β-Actin.

RNA-seq analysis

Published data were retrieved in FASTQ format from the following accession numbers: GEO GSE155176 (whole tissue transcriptome of HS lesional, HS non-lesional, and healthy skin)[25] and GSE125380 (transcriptome of total mRNA in eIF4A-inhibitor-treated mouse pancreatic ductal adenocarcinoma organoids).[26] Sequencing reads were mapped to Gencode GRCh37.hg19 and Gencode GRCm38.p4, respectively, using STAR version 2.5.2b

(options:–outReadsUnmapped Fastx; –outSAMtype BAM SortedByCoordinate; –outSAMAttributes All). Transcript abundances were calculated using Cufflinks version 2.2.1 with options–library-type fr-firststrand; -G; -L. Cuffmerge was then used to merge the transcript files from Cufflinks into one file. Following Cuffmerge, Cuffquant was used to quantify the transcript abundances, followed by differential gene expression using Cuffdiff. Differentially expressed genes with a p-value < 0.05, as well as a log2fold change >1 was analyzed further. We performed gene ontology (GO) analysis based on gene-GO association files (ftp://ftp.geneontology.org/go/gene-associations/gene_association.mgi.gz), and p-values were determined by Chi-squared test followed by Bonferroni correction.

Gene set enrichment analysis (GSEA) and ingenuity pathway analysis (IPA)

The list of 734 DEGs for eIF4F potential targets was used to analyze pathways by GSEA online tool (https://www.gsea-msigdb.org/gsea/index.jsp). We chose h.all.v7.3.symbols.gmt as the Gene sets database and Human_Gene_Symbol_with_Remapping_MSigDB.v7.4. chip as the chip platform. The integrated pathway analysis was performed using the IPA software (Qiagen, Hilden, Germany). The IPA includes a global network based on the manual curation of a vast body of medical literature and biomedical databases.

QUANTIFICATION AND STATISTICAL ANALYSIS

All data were statistically analyzed by GraphPad Prism 9.0. An unpaired two-tailed Student's *t* test was used to analyze the differences between the two groups. Differences among multiple groups were analyzed using the ANOVA test. Data are represented as mean ± standard error of the mean (SEM). Statistical significance is denoted by *$p < 0.05$, **$p < 0.01$, ***$p < 0.001$, or $^{\#\#}p < 0.005$. Detailed statistical information for relevant experiments can be found in the figures and corresponding figure legends.